Reassembly of the Dharwar and Bastar cratons at ca. 1 Ga: Evidence from multiple tectonothermal events along the Karimnagar granulite belt and Khammam schist belt, southern India

Sojen Joy[1,*], Gert Van Der Linde[1], Asru K Choudhury[2,**], Gautam K Deb[3] and Sebastian Tappe[1,4]

[1] *De Beers Group Services, Exploration, Southdale, P/Bag X01, Johannesburg 2135, South Africa.*
[2] *Indian Statistical Institute, Calcutta, India.*
[3] *Department of Geology, Presidency University, Calcutta 700 073, India.*
[4] *Department of Geology, University of Johannesburg, P.O. Box 524, Auckland Park 2006, South Africa.*
*Corresponding author. e-mail: sojen.joy@debeersgroup.com

The northern part of the Nellore–Khammam schist belt and the Karimnagar granulite belt, which are juxtaposed at high angle to each other have unique U–Pb zircon age records suggesting distinctive tectonothermal histories. Plate accretion and rifting in the eastern part of the Dharwar craton and between the Dharwar and Bastar craton indicate multiple and complex events from 2600 to 500 Ma. The Khammam schist belt, the Dharwar and the Bastar craton were joined together by the end of the Archaean. The Khammam schist belt had experienced additional tectonic events at ∼1900 and ∼1600 Ma. The Dharwar and Bastar cratons separated during development of the Pranhita–Godavari (P–G) valley basin at ∼1600 Ma, potentially linked to the breakup of the Columbia supercontinent and were reassembled during the Mesoproterozoic at about 1000 Ma. This amalgamation process in southern India could be associated with the formation of the Rodinia supercontinent. The Khammam schist belt and the Eastern Ghats mobile belt also show evidence for accretionary processes at around 500 Ma, which is interpreted as a record of Pan-African collisions during the Gondwana assembly. From then on, southern India, as is known today, formed an integral part of the Indian continent.

Keywords. U–Pb Zircon geochronology; Indian craton assembly and rifting; Rodinia; Columbia; P–G valley; Eastern Ghats Mobile Belt.

1. Introduction

It is generally accepted that the Indian subcontinent was stabilized through accretion and assembly of several Archaean nuclei, namely, the Dharwar, Aravalli–Bundelkhand, Singhbhum, and Bastar (Bhandara) cratons by c. 2.6–2.5 Ga (Radhakrishna and Naqvi 1986; Rogers 1986; Ramakrishnan and Vaidyanadhan 2008; Sharma 2009; Saha and Mazumder 2012; Jayananda *et al.*
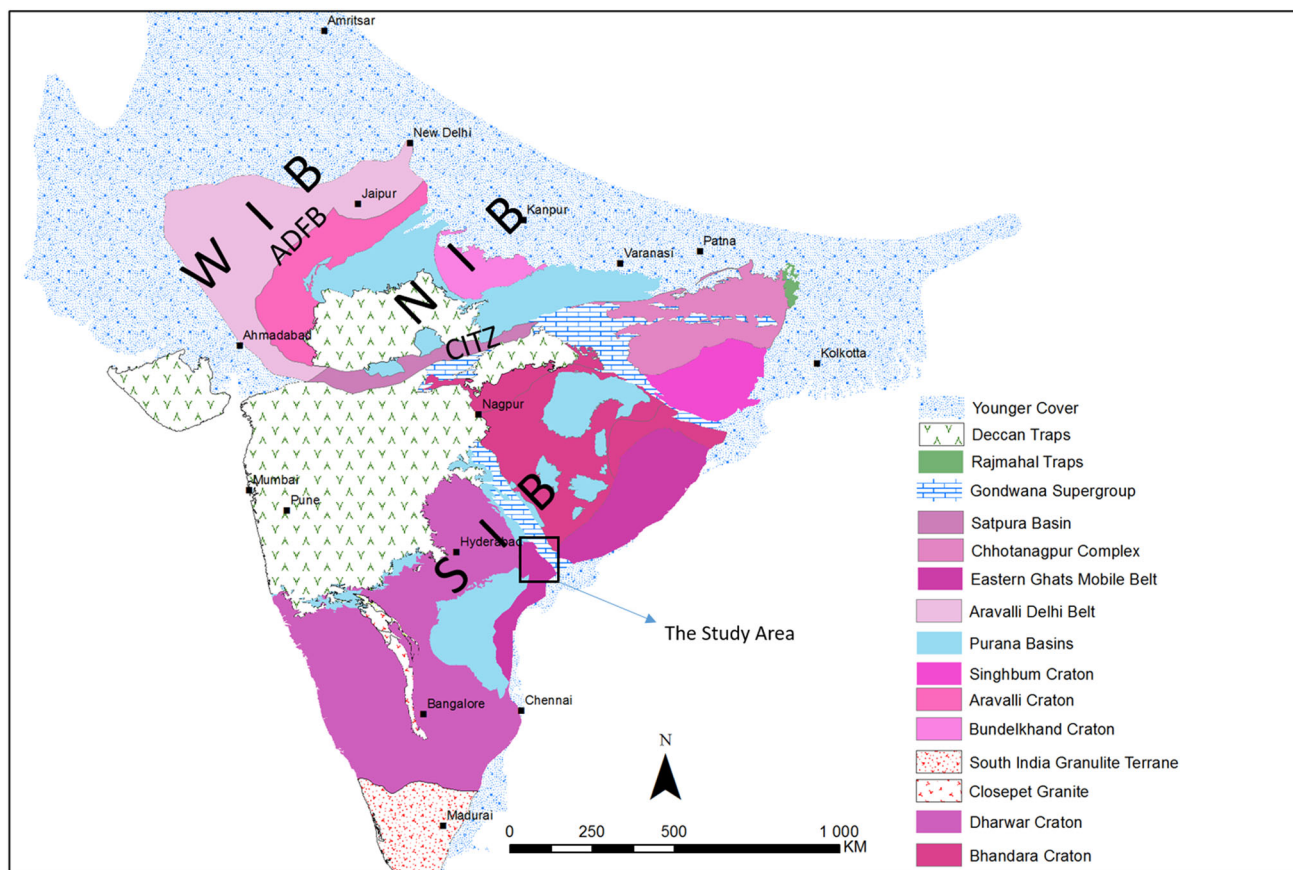

** Deceased.

Figure 1. The regional geology of India, with the WIB (western Indian block), NIB (northern Indian block), and SIB (southern Indian block), ADFB (Aravalli–Delhi fold belt) and CITZ (Central Indian Tectonic Zone) marked after Basu and Bickford (2015).

2013). Scattered across the Indian Archaean nuclei are several unmetamorphosed and only locally or weakly deformed volcano-sedimentary successions of Proterozoic age (figure 1). These erosional remnants are referred collectively in Indian literature as the 'Purana basins' (Holland 1907). Despite generally similar sedimentological features and lithofacies, as well as a similar time span of deposition between 2.0 and 0.7 Ga, the origin and evolution of these basins are not unanimously accepted (e.g., Basu and Bickford 2015; Joy *et al.* 2015; Saha *et al.* 2016).

Recently, Basu and Bickford (2015) divided the Indian continent into three main cratonic domains (southern Indian, northern Indian, and western Indian blocks – SIB, NIB and WIB, respectively; figure 1) to more readily compare the evolution of the Purana basins within the context of supercontinent development and the tectonic evolution of the Indian Proterozoic mobile belts, including the Eastern Ghats mobile belt (EGMB), the Central Indian Tectonic Zone (CITZ), and the Aravalli–Delhi fold belt (ADFB). However, it is

now well understood that the evolution of a cratonic block is constrained by the tectonic history of the constituent terranes, which differ in intensity of deformation and metamorphism. Therefore, geological and geodynamic modelling requires robust age information to assess how and when these radically different terranes had stitched into the present day cratonic configuration. Despite growing evidence of the assembly of the first supercontinent Kenorland in the Late Neoarchaean (e.g., Bradley 2011; Meert 2012; Nance and Murphy 2013; Nance *et al.* 2013), comparisons and correlations have only been made between the Neoarchaean development of the Slave province in North America, a major component of Kenorland, and the Dharwar craton of southern India (Bleeker 2003). Recently, a correlation of different stages of evolution of the Purana basins with breakup of Kenorland at ca. 2.0 Ga, reassembly of Kenorland fragments to form the Columbia supercontinent at around 1.8 Ga, fragmentation of Columbia at 1.3 Ga, and finally formation of Rodinia at 900 Ma has been made (Basu and

Bickford 2015; Saha *et al.* 2016 and references therein).

The tectono-stratigraphic development of the Nellore–Khammam schist belt (NKSB) in relation to global Proterozoic events, including possible links with the assembly of Columbia and its final dispersal, has been suggested by Saha *et al.* (2015). However, correlations between the Purana basins and the various Proterozoic mobile belts of southern India such as the Nellore–Khammam schist belt, Eastern Ghats mobile belt (EGMB) and the Karimnagar granulite belt (KGB) are unclear. Furthermore, their final incorporation into the southern Indian cratonic block (SIB) during supercontinent formation is controversially discussed (Basu and Bickford 2015).

The southern part of the SIB, comprising the western and eastern Dharwar cratons, two major Purana basins (i.e., Cuddapah basin in the south and P–G valley basin in the north), and the Nellore–Khammam schist belt, is an ideal area to test various models of supercontinent assembly, because the constituent terranes vary widely in their geographic disposition and in their stratigraphic and tectonothermal evolution. Furthermore, the SIB is bounded to the east by the Ongole domain of the EGMB, the tectonic journey with time of which is still debated. It is noteworthy that all the above-mentioned components of the SIB are bounded by discontinuities (thrust or normal faults) along their longitudinal trends. The available information on deformation features and metamorphic history indicate that they traversed differently through space and time to amalgamate at the present position. The components of the SIB could therefore be referred to as terranes.

Here we report new LA-ICP-MS U–Pb zircon ages from rocks of the Khammam schist belt and gneisses and granites within the Karimnagar granulite belt. We put forward a comprehensive picture of evolution of the SIB in the global context.

2. General geology

The geology of the study area comprises of the rocks of the Dharwar craton, the Proterozoic basins classified as part of the Purana basins of Holland (1907), the Nellore–Khammam schist belt, the Ongole and Eastern Ghats domains of the Eastern Ghats Mobile Belt (figure 2).

2.1 *Dharwar craton and Purana basins*

Based on the nature and relative abundance of greenstones, gneisses and granites the Dharwar craton has been divided into the west Dharwar craton (WDC) and the east Dharwar caton (EDC), separated by the Chitradurga Shear Zone, adjoining the western side of the Closepet Granite (Rogers 1986; Ramakrishnan and Vaidyanadhan 2008). The WDC comprises (a) older gneisses (∼3.36–3.2 Ga) with TTG affinity, which have been grouped as Peninsular Gneiss-I (Balasubrhamanyan 2006) or as Peninsular Gneiss *sensu stricto* (Chadwick *et al.* 2000), (b) two generations of greenstone belts (older Sargur Group and younger Dharwar Supergroup) and late calc-alkaline to potassic plutons (Chadwick *et al.* 2000; Jayananda *et al.* 2008, 2013). In contrast, the EDC is a juvenile Neoarchaean province characterized by linear belts and rafts of 2.7–2.55 Ga supracrustal units (greenstones) with coeval TTG gneisses and migmatites, and voluminous 2.56–2.50 Ga calc-alkaline to potassic plutonic bodies, including the prominent Closepet Granite (Chadwick *et al.* 2000; Jayananda *et al.* 2008, 2013).

All the Purana basins formed in close spatial association with the stable cratons, and at present cover collectively about 20% of the Archaean basement (Kale and Phansalkar 1991). Outcrop in and around the NW–SE trending P–G valley basin is marked by symmetrical disposition of Archaean to Mesozoic rocks. The Proterozoic Godavari Supergroup (Chaudhuri and Chanda 1991), an unmetamorphosed and locally weakly deformed sedimentary rock succession, is exposed in two linear belts along the southwestern and northeastern margins of the P–G valley, separated by a linear belt of younger Gondwana rocks (220–65 Ma; Robinson 1971). The Proterozoic belts are flanked on their outer margins by granulites and gneisses (Rajesham *et al.* 1993; Vansutre *et al.* 2013); the Karimnagar granulite belt (KGB) and the gneisses of the Dharwar craton in the SW; and the Bhopalpatnam granulite belt (BGB) and gneisses of the Bastar craton in the NE. Most of the contacts among these lithologic units are faults that follow the NW–SE trend of the P–G valley (figure 2). The P–G valley basin developed along the join between the Dharwar and Bastar cratons (Naqvi and Rogers 1987) and it is referred to as a rift basin based on geophysical and stratigraphic analyses (Qureshy *et al.* 1968; Naqvi *et al.* 1974; Chaudhuri *et al.* 2002). However, there
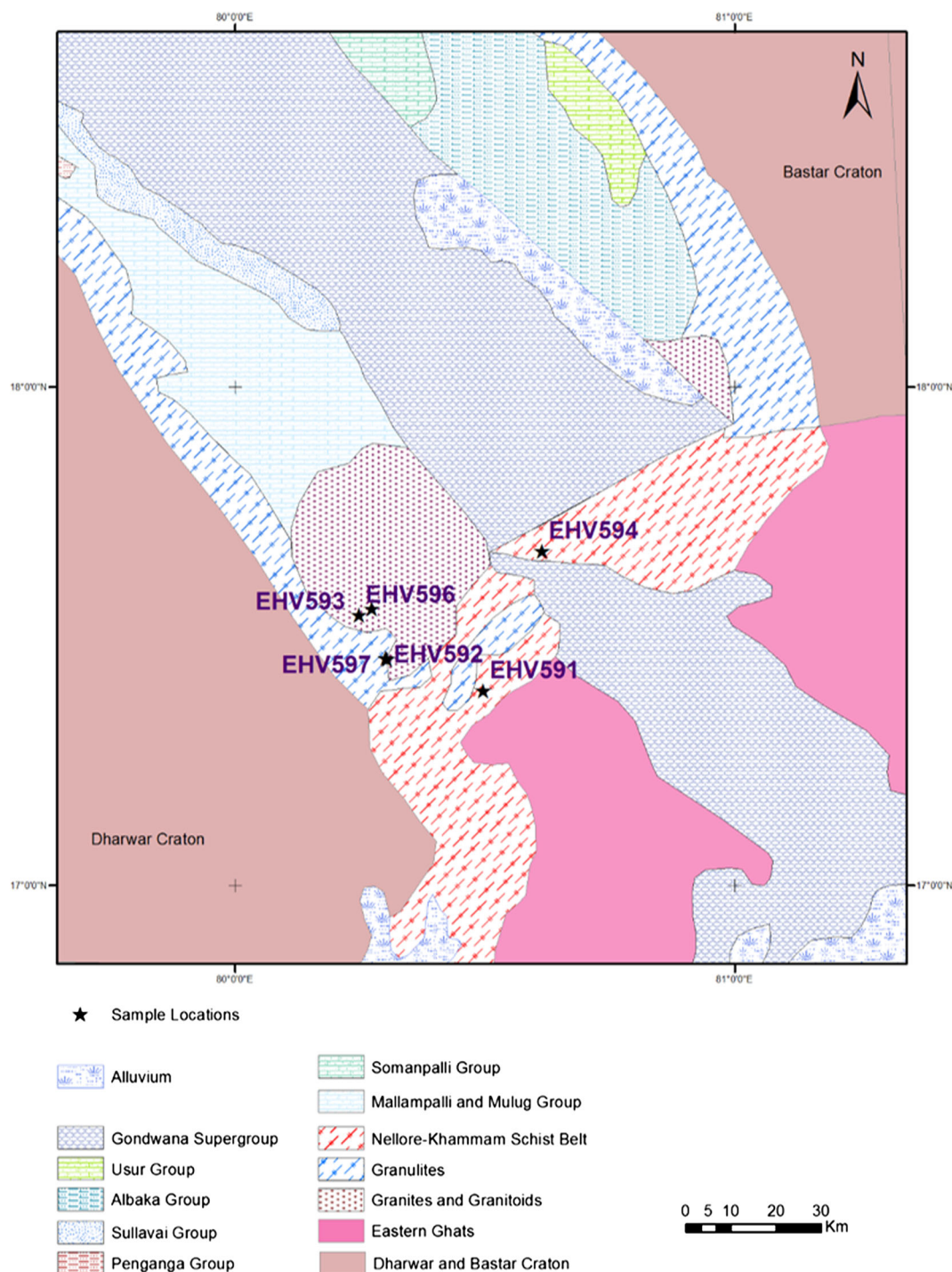
Figure 2. Geological map of the study area (modified after Chaudhuri *et al.* 2012) showing the location of the samples collected. The unit which was mapped as unclassified by Chaudhuri *et al.* (2012), was later classified as granitites and granitoids (Chaudhuri and Deb, personal communication).

are alternative tectonic models that view the evolution of the Purana basins as foreland and sag basins (e.g., Acharyya 2003; Basu and Bickford 2015).

The other Proterozoic basin of the SIB is the oval shaped Cuddapah basin, the largest among all Purana basins, which hosts 1.9 Ga and younger unconformity-bound sedimentary rock successions (Saha and Tripathy 2012; Saha and Patranabis-Deb 2014; Saha *et al.* 2016). The eastern part of the basin evolved into the Mesoproterozoic Nallamalai fold-thrust belt, whereas the undeformed sedimentary rock successions in the west rest unconformably on the EDC gneisses.

2.2 *Nellore–Khammam schist belt*

The Nellore–Khammam schist belt (NKSB) is about 600 km long and 30–130 km wide (Hari Prasad *et al.* 2000). Its major southern extension (Nellore schist belt) separates the intracratonic Cuddapah basin to the west and the Ongole domain of the Eastern Ghats belt. In the northern extension, close to the P–G valley basin, the belt is referred to as the Khammam schist belt (Ramam and Murty 1997; Hari Prasad *et al.* 2000; Okudaira *et al.* 2001; Saha *et al.* 2015), where it is sandwiched between the EGMB and the Proterozoic sedimentary succession of P–G valley. The NKSB consists of several geologically and geochemically distinct volcano-sedimentary successions named the Vinjamuru Group, Kandra ophiolite complex (KOC), Kanigiri ophiolitic melange (KOM) and Udaigiri Group (Saha *et al.* 2015; Sain *et al.* 2017).

The Udaigiri Group is composed of predominantly greenschist facies metasedimentary rocks, whereas the Vinjamuru Group is dominantly an amphibolite facies volcano-sedimentary assemblage (Moeen 1998; Dobmeier and Raith 2003). There are two ophiolite complexes reported from the schist belt, namely the Kandra ophiolite complex (Vijaya Kumar *et al.* 2010) in the southern part and the Kanigiri ophiolite melange (Dharma Rao *et al.* 2011a) in the central part of the NKSB. The NKSB rocks show multiple deformation and metamorphism, as well as emplacement of granites and alkaline plutons (Saha *et al.* 2015 and references therein). Dobmeier and Raith (2003) grouped the granulite facies rocks of the Ongole domain to the NKSB and classified them as the Late Paleoproterozoic Krishna province, distinct from the Mesoproterozoic Eastern Ghats province. In contrast, Saha *et al.* (2015) proposed a Late Neoarchaean to Mesoproterozoic development of the NKSB independent of the Eastern Ghats belt. Although Ramakrishnan (2003) emphasised differences in tectono-stratigraphic features between the EDC greenstone belts and the Nellore–Khammam schist belt, this schist belt is often considered as the easternmost greenstone belt of the eastern Dharwar craton (Vadlamani 2010).

2.3 *Karimnagar and Bhopalpatnam granulite belts*

As mentioned earlier, the Dharwar and Bastar cratons are juxtaposed along a NW–SE trending join that was the keel of the P–G valley basin bordered by the Karimnagar and Bhopalpatnam

granulites belts (KGB and BGB) to the southwest and northeast, respectively (figure 2). These granulites occur as several enclaves and discrete narrow bands mixed with granites, granite gneisses and amphibolites (Rajesham *et al.* 1993; Santosh *et al.* 2004; Vansutre *et al.* 2013). We use the term KGB to include all these units in a tectono-stratigraphic sense.

Both granulite belts have characteristic length: width ratios of at least 5:1. The Karimnagar granulite belt (KGB) is interpreted as an Archaean supracrustal-granite association, metamorphosed to granulite grade, representing the suture zone between the Dharwar and Bastar cratons (Rajesham *et al.* 1993). The KGB is characterised by at least two phases of deformation resulting in near isoclinal refolding with axial planar cleavages and the tectonothermal events in KGB match with those in the eastern Dharwar craton (Rajesham *et al.* 1993). The 300-km long Bhopalpatanam granulite belt (BGP) lies on the western edge of the Bastar craton (figure 2) and is composed of two pyroxene granulites, ultramafics, quartzite, calcsilicate rocks, Mg–Al metapelites (Vansutre and Hari 2010). The peak metamorphic condition of the high Mg–Al granulite within the KGB is estimated as 7.5–8 kb at 800–840°C (Prakash *et al.* 2017).

2.4 *Eastern Ghats mobile belt*

The Eastern Ghats mobile belt (EGMB), follows the east coast of India for over 1000 km adjoining the Dharwar, Bastar and Singhbhum cratons to the east. The EGMB is considered as an exotic distal Grenvillian terrane, juxtaposed to the Indian continent (Chaudhuri *et al.* 2012). The belt is a composite of accreted linear continental and oceanic fragments of moderate to high metamorphic grade, including granulite facies rocks, which have been intruded by suites of granites, anorthosites and nepheline syenites. A terrane boundary shear zone marks the juxtaposition of the EGMB with the Indian cratons, which is of strike slip character in the north and thrust character in the west and southwest (Ratre *et al.* 2010). The EGMB is divided into four provinces: the Jaypore province, the Rengali province, the Eastern Ghats province and the Krishna province, each with distinct tectonothermal histories (Dobmeier and Raith 2003). The Jaypore and Rengali Province accreted to proto-India prior to the 1000 Ma assembly of Rodinia (Mukhopadhyay and Basak 2009). The Eastern Ghats province

records high grade metamorphism and orogenesis at 980–930 Ma during amalgamation of Rodinia (Korhonen *et al.* 2011). The Krishna Province records collisional orogenesis and high temperature metamorphism at 1600 Ma (Dobmeier and Raith 2003; Upadhyay *et al.* 2009; Henderson *et al.* 2013). The Krishna province is divided into the Ongole domain in the east and NSB in the west, which has been refuted by Saha *et al.* (2015), as discussed above in section 2.2, considering only the Ongole domain to be part of the EGMB.

3. Previous geochronology work

Geochronological data from different terranes of the SIB have enhanced our knowledge about many tectonothermal events of southern India. However, a more detailed data synthesis is presented below to better understand the evolution of the SIB.

3.1 *Purana basins and eastern Dharwar craton*

The EDC is composed of number of greenstone belts of Neoarchaean age (2700–2500 Ma) (Jayananda *et al.* 2013 and references therein). The Closepet Granite (2513±5 Ma; Friend and Nutman 1991; Jayananda *et al.* 2013) and equivalents form a widespread Neoarchaean plutonic phase in the Dharwar craton. It has been suggested that emplacement of the Closepet Granite represents the amalgamation of the WDC and EDC at ∼2.5 Ga (Jayananda *et al.* 2013).

Previous geological mapping combined with recent geochronological studies conducted on the Purana basin rocks suggest that deposition in these basins started as early as 1.9 Ga (Cuddapah basin) and basin evolution possibly ended at <1.0 Ga (Rasmussen *et al.* 2002; Ray *et al.* 2002; Patranabis-Deb *et al.* 2007; Malone *et al.* 2008; Das *et al.* 2009; Conrad *et al.* 2011; Sheppard *et al.* 2017). The Sullavai sedimentation continued until about 720 Ma or beyond in the P–G valley (Joy *et al.* 2015). However, the exact ages of the youngest sedimentary sequences in each of the basins are only poorly constrained.

The post-cratonization events in the EDC are composed of mafic dykes, kimberlites and lamproites. Protracted period of dyke activity (2.4–1.1 Ga) is reported from the EDC (table 1). Age of the kimberlites cluster around 1100 Ma and the lamproites in the Nallamalai fold belt at around 1400 Ma (Kumar *et al.* 2007; Chalapathi Rao *et al.* 2013;

Chalapathi Rao and Srivastava 2016 and references therein).

3.2 *Nellore–Khammam schist belt*

3.2.1 *Vinjamuru Group*

Sm–Nd isotope analysis from the Vinjamuru gabbro of the NKSB has yielded 2654±100 Ma whole rock age and a 1911±88 Ma isochron age (Vadlamani 2010). The data has been interpreted by Vadlamani (2010) to imply that the 2.7 Ga old NKSB was intruded by MORB-type gabbro at 1911 Ma in response to a major extensional event along the east Dharwar craton margin. The geochemical and geochronological evidences led (Vadlamani 2010) to consider the volcanic events at ∼1.9 Ga in the NKSB and Cuddapah basin (mafic–ultramafic sills, and gabbroic intrusives) as representing a single large anorogenic igneous event in the eastern Dharwar craton and NKSB. The andesites and rhyolites of the Vinjamuru Group have been dated through zircon Pb evaporation methods to be ∼1868 and 1771–1791 Ma, respectively (Vadlamani *et al.* 2012) and the authors propose that this volcanism occurred during a major convergent orogenic event along the southeastern margin of the eastern Dharwar craton.

The Vinukonda Granite intrusive to the Vinjamuru Group is dated as ∼1590 Ma (U–Pb zircon TIMS; Dobmeier *et al.* 2006), and represents the minimum age of the Vinjamuru Group.

Ghosh *et al.* (1994) report fission track and K–Ar dates showing pegmatite events at 1600, ∼1000 and 600±100 Ma from the Nellore mica belt (in the southern part of NKSB). The ∼500 Ma event is also represented by the phengite Rb–Sr ages from mylonites of the Vinukonda granite (Dobmeier *et al.* 2006).

Dharma Rao *et al.* (2011b) report an Sm–Nd model age of ∼1170 Ma from the Chimalpahad anorthosite complex in the NKSB and interpret it as an accreted arc fragment within the NKSB.

Yoshida *et al.* (1996) reported 1126 Ma from metapelite from the Khammam area based on an Pb–Pb mineral isochron. Okudaira *et al.* (2001), based on an Sm–Nd mineral isochron from amphibolites of the Khammam schist belt, proposed 824±53 Ma as the age of metamorphism of the Khammam schist belt and interpreted to be the result of the tectonic accretion of the EGMB to the Dharwar–Bastar craton. Okudaira *et al.* (2001) also report another thermal event from the

Table 1. *Summary of geochronology reported for dykes in the EDC.*

Age	Name of dyke	Method	Reference
1192 Ma	Bangalore, N–W alkaline dykes	U–Pb Zircon LA–MC–ICPMS	Pradhan *et al.* (2008)
1500–1350 Ma	Anantapur ENE–WSW dykes	K–Ar	Murthy *et al.* (1987), Mallikarjuna *et al.* (1995)
1900–1700 Ma	Anantapur NE–SW dykes	^{40}Ar–^{39}Ar	
2081±4 Ma	Radial dykes Cuddapah basin flanks	Pb–Pb TE–TIMS and U–Pb ID–TIMS baddeleyite age	Kumar *et al.* (2015), Demirer (2012)
2.1–2.0 Ga	Anantapur dykes	U–Pb zircon, LA–ICPMS	Belica *et al.* (2014)
2173 + 64 Ma	Mahabubnagar gabbros, dolorites and pyroxenites	Sm–Nd, U–Pb zircon and baddeleyite,	Pandey *et al.* (1997), French *et al.* (2004)
~ 2180 Ma			
2.2 Ga	Tirupathi dykes	U–Pb zircon and baddeleyite, ID–TIMS	French and Heaman (2010)
2370–2365 Ma	Bangalore, E–W dolerites	U–Pb Zircon, ID–TIMS and U–Pb baddeleyite	French *et al.* (2004), Halls *et al.* (2007)
2.4–2.2 Ga	Hyderabad dolerites	U–Pb ID–TIMS baddeleyite ages	Kumar *et al.* (2012a,b)

same rocks at 481±16 Ma using a Rb–Sr mineral isochron.

3.2.2 *Kandra ophiolite complex (KOC) and Kanigiri ophiolitic melange (KOM)*

The Kandra ophiolite complex is dated as around 1850–1900 Ma (SHRIMP U–Pb zircon ages by Vijaya Kumar *et al.* (2010) and Sm–Nd isochron age by Vadlamani (2010)). The Kanigiri complex is dated at around 1330 Ma (LA-ICP-MS U–Pb zircon ages by Dharma Rao *et al.* 2011a). The timing of the post orogenic granite emplacement in the KOM is defined by the A-type Kanigiri granite intruding the KOM, dated at 1284 Ma (Sain *et al.* 2017). There is a 500 My age difference between these two ophiolite complexes and their history is proposed as an example of accretion along a craton margin over a prolonged period of convergence (Dharma Rao *et al.* 2011a). Saha (2011) proposed multiple cycles of ophiolite emplacement based on the divergent nature of thrusting in the area.

3.2.3 *Udaigiri Group and Prakasam alkaline complex*

The only age available from the Udaigiri Group is very poorly constrained at 1929±130 Ma based on a single grain xenotime analysis by Das *et al.* (2015).

The Prakasam alkaline plutons occurring along the boundary between the Vinjamuru and Ongole domains are dated by various methods at between 1242 and 1369 Ma (Upadhyay 2008 and references therein), interpreted to represent the rifting during the breakup of Columbia (Upadhyay 2008).

3.3 *Karimnagar and Bhopalpatnam granulite belts*

Santosh *et al.* (2004) report zircon (EPMA) ages from the KGB with the cores recording ages of up to 3.1 Ga and rims with ages of 2.6 Ga. In contrast, the cores of zircons recovered from the BGB demonstrate core ages of 1.9 Ga and the rims of 1.6–1.7 Ga. The monazites from the BGB also record the 1600±3 Ma age, interpreted as the most important tectonothermal event in the BGB. As there are no Mesoproterozoic tectonothermal events recorded from the KGB, the KGB and BGB are interpreted to have experienced different P–T conditions at different times (Santosh *et al.* 2004). The authors also note that the 1600 Ma age is not recorded from the KGB nor from

Table 2. *Details of the samples collected.*

Sample no.	Geology	Rock type	Minerals	Longitude	Latitude	Sample description
EHV597	Karimnagar granulite belt	Augen Gneiss	Qtz+Kfs+Pl+Ms+Bt+Opx+Ep+Zr+Ap+Op	80.30222	17.45583	Augen gneiss, black in colour due to relatively fine grain size as well as abundance of biotite. Grain size reduction was possibly due to dynamic recrystallization in relation to intense shearing
EHV592	Karimnagar granulite belt	Banded Gneiss	Qtz+Pl+Kfs+Opx+Bt+Sp+Zr+Ap+Op+Mz	80.30472	17.45333	Banded gneiss which occurs as large lenticular body within the augen schist country rock. Up to 2 cm thick and alternating quartz-feldspar-rich and quartz-feldspar-poor bands are present. Tight to isoclinal folds on the banding occur, and the axial planes are nearly parallel to the schistosity of the enclosing augen schist. The sample is interpreted as a xenolith or enclave in the augen schist country rock
EHV596	Karimnagar granulite belt	Foliated granite	Qtz+Kfs+Pl+Grt+Bt+Zr+Ap+Op	80.24917	17.54278	Foliated granite outcrop with abundant xenoliths of amphibolite and other basic dykes. There are xenoliths with the granite schist, especially with sharp contacts with the granite schist, especially where the schistosity is deflected around the xenoliths. In other places, contact between the two rock types is rather gradational, and interleaving between the basic rocks and the granitic material is evident
EHV593	Karimnagar granulite belt	Schistose granite	Qtz+Kfs+Pl+Grt +Ms+Chl+Ep+Zr	80.27444	17.55528	Schistose granite with 1 to 2 cm large megacrysts/porphyroblasts (augen) of pink feldspar surrounded by the mylonitic foliation defined by recrystallized quartz and feldspar grains, as well as biotite flakes. The schistose granite is part of a shear zone bordering the PG Valley
EHV594	Nellore–Khammam schist belt	Augen gneiss	Qtz+Kfs+Pl+Grt+Ms+Ep+Zr+Ap+Op	80.61556	17.67139	Gneiss with augen of pink feldspar, strongly sheared with prominent mylonitic foliation. The gneiss occurs as an intrusive body within garnet-bearing mica schist
EHV591	Nellore–Khammam schist belt	Quartzo feldspathic gneiss	Qtz+Kfs+Pl+Hbl+Grt+Bt+Zr	80.49722	17.39083	Quartz-feldspar-biotite gneiss with alternating quartz-feldspar-rich and biotite-rich bands. Occurrence of metamorphic garnet indicates a metasedimentary protolith
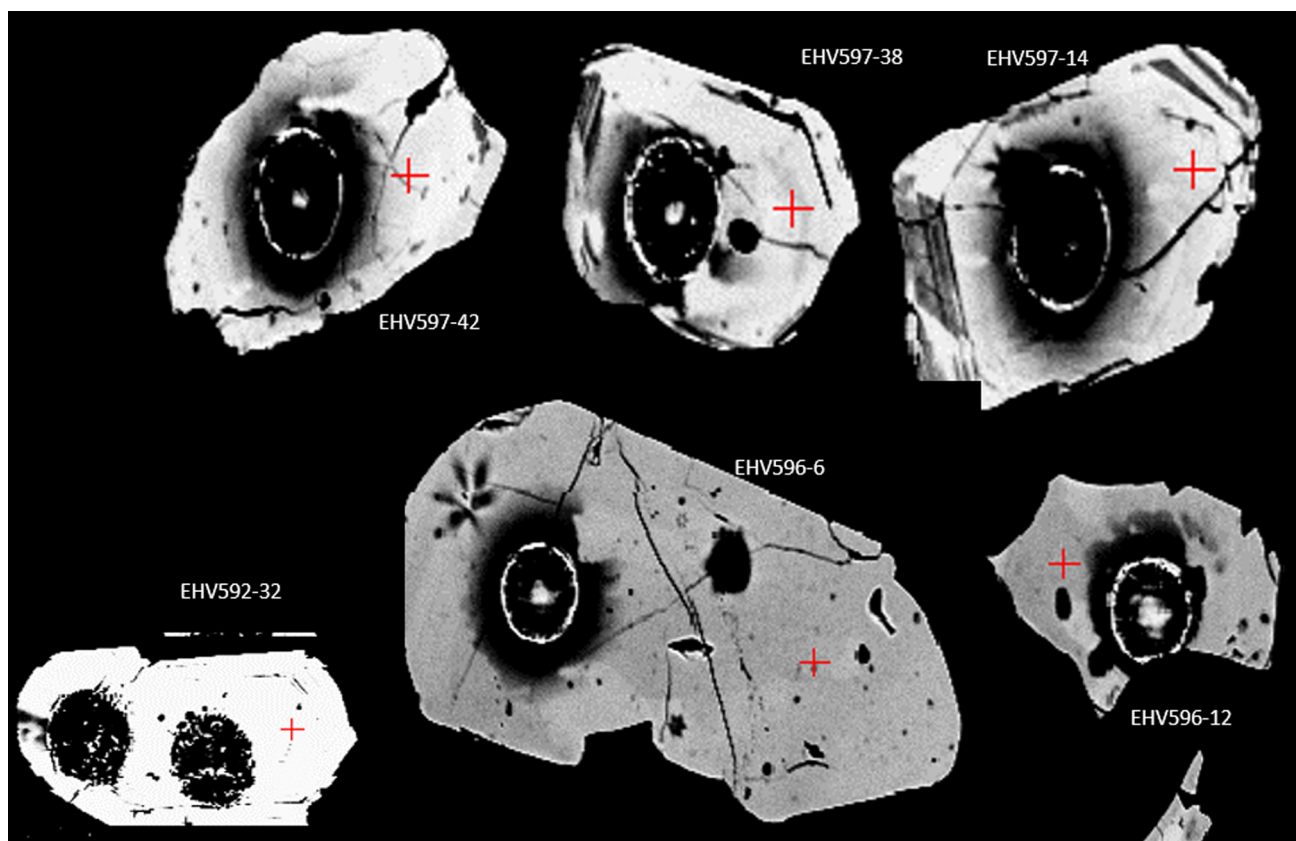
Figure 3. Examples of back scatter electron Z images captured using a CAMECA SX100 Electron Probe Micro Analyser for samples from the Karimnagar granulite belt. Ablation spots are 35 µm in diameter and can be seen as circular holes.

the Bastar craton. Santosh *et al.* (2004) further note the absence of Grenvillian (ca. 1000 Ma) and Pan-African (ca. 520–550 Ma) ages from the KGB and suggest that the KGB was not directly involved in these younger collisional events that led to supercontinent amalgamation. The peak metamorphic age of the high Mg–Al granulite in the KGB the area has been recently reported by Prakash *et al.* (2017) as 2604±25 Ma (SHRIMP U–Pb zircon).

Granites intruding the supracrustal belt in the KGB are dated as 2490±115 Ma (Rb–Sr whole rock; Crawford 1969). This event is probably linked to the rim ages reported by Santosh *et al.* (2004) in the zircons.

3.4 *Eastern Ghats mobile melt*

The Jaypore and Rengali provinces accreted to proto-India prior to the 1000 Ma assembly of Rodinia (Mukhopadhyay and Basak 2009; Dasgupta *et al.* 2017). The EG province records high grade metamorphism and orogenesis at 980–930 Ma (SHRIMP U–Pb monazite dating) during

amalgamation of Rodinia (Korhonen *et al.* 2011). The Ongole domain records collisional orogenesis and high temperature metamorphism at 1600 Ma (Dobmeier and Raith 2003; Upadhyay *et al.* 2009; Henderson *et al.* 2013).

The crystallization of charnockites and enderbites in the centre of the Ongole domain is dated at 1720–1700 Ma (Kovach *et al.* 2001). The deposition of the sedimentary protolith in the Ongole domain is reported to be during 1.72–1.68 Ga and based on the U–Pb and Lu–Hf data has been proposed not to be sourced from the Dharwar craton, but from the Napier Complex in Antarctica (Henderson *et al.* 2013). A small proportion of pre-Neoarchaean detrital zircons from the Ongole domain is also reported by Henderson *et al.* (2013). The granulite facies metamorphism in the Ongole domain is dated as 1.68–1.6 Ga (Henderson *et al.* 2013). It has been proposed that the Ongole domain accreted to proto-India during 1.68–1.6 Ga, as part of a linear accretionary orogenic belt (Henderson *et al.* 2013).

North of the Godavari Rift the granulite metamorphism and magnetism are mainly in the interval

Table 3. *Results of U–Pb analysis of the zircons from sample EHV597 from the KGB.*

	Grain-ID	$^{207}Pb/^{235}U$	2σ	$^{206}Pb/^{238}U$	2σ	$^{207}Pb/^{235}U$ (Age)	1σ	$^{206}Pb/^{238}U$ (Age)	1σ	$^{207}Pb/^{206}Pb$ (Age)	1σ	Disc (%)	Pb (ppm)	Th (ppm)	U (ppm)	Th/U	Accepted age	1σ
1	EHV597-01	3.695	0.178	0.277	0.007	1570.3	19.3	1578.2	18.9	1598.2	31.6	1.3	175.68	897.25	689.75	1.3	1578.2	18.85
2	EHV597-02	3.260	0.173	0.248	0.007	1471.5	20.6	1430.5	17.5	1582.6	33.8	9.6	114.76	436.33	502.99	0.9	1430.5	17.47
3	EHV597-03	3.807	0.177	0.283	0.008	1594.2	18.7	1605.0	19.0	1568.3	31.0	−2.3	249.05	660.54	959.17	0.7	1594.2	18.68
4	EHV597-04	3.802	0.212	0.273	0.007	1593.1	22.4	1554.0	18.9	1608.4	34.2	3.4	108.71	250.9	434.12	0.6	1554	18.85
5	EHV597-05	3.601	0.178	0.277	0.007	1549.7	19.6	1574.2	18.8	1573.3	32.2	−0.1	179.96	485.26	708.21	0.7	1574.2	18.8
6	EHV597-06	3.315	0.193	0.251	0.007	1484.5	22.8	1444.3	17.8	1600.4	35.9	9.8	111.73	231.59	484.21	0.5	1444.3	17.81
7	EHV597-07	3.432	0.195	0.256	0.007	1511.8	22.4	1470.6	18.0	1590.1	35.3	7.5	120.67	361.98	512.47	0.7	1470.6	18
8	EHV597-08	3.891	0.179	0.277	0.007	1611.7	18.6	1574.6	18.6	1581.6	31.0	0.4	355.62	1765.43	1398.46	1.3	1611.7	18.61
9	EHV597-09	1.871	0.334	0.178	0.007	1070.8	59.1	1056.3	20.4	1089.5	114.9	3.0	10.49	5.19	64.06	0.1	1056.3	20.4
10	EHV597-10	1.787	0.208	0.163	0.005	1040.7	37.9	971.1	15.0	1026.4	78.6	5.4	25.3	45.65	169.3	0.3	971.1	14.96
11	EHV597-11	3.587	0.205	0.268	0.007	1546.5	22.7	1528.5	18.6	1571.7	35.5	2.7	120.92	655.84	491.39	1.3	1528.5	18.57
12	EHV597-12	3.824	0.184	0.298	0.008	1597.8	19.4	1681.8	19.8	1529.3	32.3	−10.0	272.61	204.88	994.37	0.2	1597.8	19.39
13	EHV597-13	3.720	0.208	0.272	0.007	1575.7	22.4	1548.7	18.7	1593.5	34.9	2.8	137.42	281.62	550.15	0.5	1548.7	18.7
14	EHV597-14	3.517	0.220	0.267	0.007	1531.0	24.7	1527.1	18.8	1544.9	38.0	1.2	89.49	296.82	363.9	0.8	1527.1	18.76
15	EHV597-16	2.883	0.159	0.230	0.006	1377.5	20.8	1333.9	16.4	1483.8	36.4	10.1	103.98	131.43	491.54	0.3	1333.9	16.36
16	EHV597-17	3.656	0.215	0.275	0.008	1561.8	23.5	1563.7	19.0	1575.6	36.5	0.8	87.58	401.06	346.65	1.2	1563.7	18.95
17	EHV597-19	3.184	0.150	0.249	0.007	1453.4	18.2	1434.8	17.1	1568.3	32.7	8.5	315.79	1267.87	1376.02	0.9	1434.8	17.1
18	EHV597-20	3.276	0.198	0.251	0.007	1475.4	23.5	1446.2	17.8	1581.4	37.8	8.5	82.85	193.69	357.79	0.5	1446.2	17.77
19	EHV597-21	3.668	0.209	0.284	0.008	1564.5	22.7	1611.2	19.3	1537.9	36.4	−4.8	151.8	556.28	580.45	1.0	1611.2	19.31
20	EHV597-23	3.994	0.228	0.284	0.008	1633.0	23.2	1611.0	19.3	1615.4	36.0	0.3	150.99	609.77	577.26	1.1	1611	19.28
21	EHV597-24	3.581	0.234	0.268	0.007	1545.3	25.9	1530.7	18.9	1603.7	39.7	4.6	120.22	528.24	486.79	1.1	1530.7	18.85
22	EHV597-26	3.939	0.224	0.287	0.008	1621.7	23.0	1627.5	19.4	1582.9	36.5	−2.8	180.02	559.54	680.07	0.8	1627.5	19.41
23	EHV597-28	3.599	0.207	0.261	0.007	1549.4	22.8	1493.6	18.1	1612.0	37.0	7.3	147.63	322.74	614.19	0.5	1493.6	18.05
24	EHV597-30	3.777	0.232	0.286	0.008	1587.9	24.7	1619.5	19.5	1529.8	38.9	−5.9	102.18	363.86	387.95	0.9	1619.5	19.52
25	EHV597-32	3.366	0.201	0.257	0.007	1496.6	23.4	1474.0	17.9	1529.6	39.1	3.6	117.3	452.61	494.92	0.9	1474	17.9
26	EHV597-33	3.362	0.193	0.251	0.007	1495.5	22.5	1441.1	17.4	1564.1	38.2	7.9	142.09	928.73	614.67	1.5	1441.1	17.44
27	EHV597-35	3.720	0.231	0.274	0.007	1575.7	24.9	1560.1	18.9	1521.2	40.1	−2.6	125.19	475.49	495.34	1.0	1560.1	18.87
28	EHV597-37	3.563	0.205	0.276	0.007	1541.4	22.9	1570.5	18.8	1536.6	38.9	−2.2	197.43	462.17	775.09	0.6	1570.5	18.78
29	EHV597-38	3.253	0.221	0.242	0.007	1469.9	26.4	1396.2	17.4	1562.8	43.1	10.7	99.86	449.38	447.14	1.0	1396.2	17.42
30	EHV597-40	3.394	0.227	0.252	0.007	1503.0	26.3	1448.4	17.9	1539.2	42.9	5.9	109.55	502.89	470.75	1.1	1448.4	17.9
31	EHV597-41	3.274	0.231	0.244	0.007	1474.8	27.4	1405.4	17.6	1509.8	44.9	6.9	81.23	250.22	360.81	0.7	1405.4	17.59
32	EHV597-42	3.525	0.237	0.278	0.008	1532.9	26.6	1578.8	19.3	1547.5	43.3	−2.0	115.33	500.4	449.65	1.1	1578.8	19.31
33	EHV597-43	3.571	0.231	0.268	0.007	1543.1	25.7	1530.5	18.7	1567.9	42.4	2.4	100.86	388.19	407.17	1.0	1530.5	18.65
34	EHV597-44	3.718	0.215	0.278	0.007	1575.2	23.1	1579.3	18.8	1559.4	40.1	−1.3	224.18	303.03	873.43	0.3	1579.3	18.82
35	EHV597-45	3.788	0.241	0.277	0.008	1590.2	25.5	1575.1	19.0	1567.6	42.1	−0.5	122.59	159.61	478.99	0.3	1575.1	19.03
36	EHV597-47	1.690	0.215	0.166	0.006	1004.8	40.6	991.6	15.8	1008.4	87.4	1.7	17.63	9.19	114.59	0.1	991.6	15.77
37	EHV597-50	3.554	0.230	0.279	0.008	1539.4	25.7	1587.7	19.2	1537.5	43.8	−3.3	133.04	628.25	514.71	1.2	1587.7	19.22

No	Sample																	
38	EHV597-52	1.361	0.147	0.145	0.005	872.5	31.7	873.1	13.1	899.6	80.3	2.9	22.74	22.78	169.34	0.1	873.1	13.1
39	EHV597-54	3.438	0.232	0.255	0.007	1513.0	26.6	1461.9	18.0	1535.0	45.8	4.8	131.91	694.73	559.42	1.2	1461.9	17.97
40	EHV597-55	1.616	0.185	0.158	0.005	976.5	35.9	947.5	14.3	922.7	82.1	−2.7	24.16	23.83	164.66	0.1	947.5	14.29
41	EHV597-25	3.747	0.227	0.297	0.008	1581.6	24.3	1677.1	20.1	1499.8	38.3	−11.8	122.73	402.2	448.18	0.9	NA	NA
42	EHV597-48	3.498	0.217	0.249	0.007	1526.9	24.5	1433.1	17.5	1617.2	42.1	11.4	209.01	783.62	907.4	0.9	NA	NA
43	EHV597-46	3.145	0.214	0.236	0.007	1443.8	26.2	1363.8	17.0	1550.8	44.6	12.1	86.07	345.04	394.99	0.9	NA	NA
44	EHV597-29	3.188	0.186	0.237	0.006	1454.2	22.5	1373.3	16.8	1594.9	37.9	13.9	112.05	329.24	511.86	0.6	NA	NA
45	EHV597-49	3.139	0.213	0.232	0.006	1442.3	26.1	1346.1	16.8	1576.6	44.9	14.6	118.63	478.8	552.07	0.9	NA	NA
46	EHV597-36	3.116	0.194	0.232	0.006	1436.7	23.9	1345.5	16.6	1584.1	40.6	15.1	105.91	572.27	494.27	1.2	NA	NA
47	EHV597-34	3.009	0.177	0.224	0.006	1409.8	22.4	1303.0	16.0	1568.8	39.2	16.9	125.94	585.12	609.15	1.0	NA	NA
48	EHV597-15	3.246	0.188	0.232	0.006	1468.3	22.5	1347.3	16.6	1643.5	36.2	18.0	80.33	418.58	375.59	1.1	NA	NA
49	EHV597-51	1.674	0.201	0.157	0.005	998.6	38.1	942.3	14.8	1158.8	82.0	18.7	14.12	10.53	96.9	0.1	NA	NA
50	EHV597-22	3.079	0.198	0.219	0.006	1427.4	24.6	1278.3	16.1	1604.2	39.8	20.3	96.16	449.98	475.99	0.9	NA	NA
51	EHV597-39	2.005	0.291	0.166	0.006	1117.2	49.2	990.7	17.0	1260.5	91.1	21.4	20.02	13.52	130.47	0.1	NA	NA
52	EHV597-18	2.407	0.141	0.184	0.005	1244.7	21.0	1088.1	13.8	1573.2	38.3	30.8	87.29	364.48	515.7	0.7	NA	NA
53	EHV597-31	2.345	0.144	0.173	0.005	1226.2	21.9	1027.1	13.1	1649.3	40.6	37.7	87.37	505.1	548.37	0.9	NA	NA
54	EHV597-53	2.291	0.221	0.158	0.005	1209.4	34.1	947.2	13.8	1724.6	59.6	45.1	28.29	23.82	192.98	0.1	NA	NA

NA: Not Applicable. Bold data are rejected and not utilised in the analysis. Discordance is defined as $1 - (^{206}\text{Pb}/^{238}\text{U Age} \div {}^{207}\text{Pb}/^{206}\text{Pb Age})$.

1.1–1.0 Ga and define the connection of EGMB with the Reyner–Napier complex of the Eastern Antarctica during the assembly of Rodinia (Rickers *et al.* 2001; Dobmeier and Raith 2003; Henderson *et al.* 2013; Dasgupta *et al.* 2017; Meert *et al.* 2017).

Saha *et al.* (2015) postulate long term episodic growth of the eastern craton margin of India in the Proterozoic, culminating in the final docking of the EGMB at ∼500 Ma (also Biswal *et al.* 2007; Vijaya Kumar and Leelanandam 2008).

4. Methodology

4.1 *Sampling*

Samples (∼5 kg) of granite and gneiss were collected from the southeastern portion of the P–G valley basin close to the boundary with the Eastern Ghats domain, which tectono-stratigraphically belongs to the Karimnagar granulite belt and the Khammam schist belt, i.e., the northern part of NKSB (table 2 and figure 2).

4.2 *Analytical method*

The samples were concentrated at the De Beers sample treatment centre, Bangalore, India. The treatment process consisted of crushing, screening, standard dense media separation (DMS), low intensity magnetic separation and heavy liquid separation through a lithium heteropolytungstate solution (LST). The resultant heavy mineral concentrate was partitioned to two size fractions, viz., (+0.3–0.5 mm) and (+0.5–1.0 mm). The zircons were identified visually under binocular microscopes and analysed at the De Beers Exploration Indicator Mineral Laboratory (DBE IML), Johannesburg. The handpicked zircons were mounted in 25 mm diameter epoxy mounts and polished to fully expose the midsection of the grains. Epoxy mount surfaces were cleaned using 96% ethanol and were put in a vacuum chamber to ensure sufficient outgassing of the epoxy.

The U–Pb isotope analyses were done at the DBE IML, using a New Wave 193 Excimer laser ablation system equipped with a Large Format ablation cell and interfaced with a Thermo Fisher X-Series 2 quadrupole ICP-MS. The ICP-MS instrument was optimised for maximum sensitivity, stability and low background using the NIST-610 glass standard. Ablations were carried out in a helium atmosphere, with a laser spot size of

35 µm. Ablation sites were placed at the centre of the zircon grains and away from cracks. Due to the small grain size, only one spot analysis was carried out per grain and it was not possible to carry out analyses of thin zircon rims. Unknowns and standards were ablated for 60 sec, followed by generous washouts of 5 min. The masses ^{206}Pb, ^{207}Pb, ^{208}Pb, ^{235}U, ^{238}U and ^{232}Th were measured for 50 ms each, yielding a total sweep time of 300 ms. Data reduction was done using the GLITTER Laser Ablation data reduction software (Van Achterbergh *et al.* 2001). The GJ-1 zircon standard (slightly discordant, ID-TIMS ^{207}Pb/^{206}Pb age 608.5±0.4 Ma, Jackson *et al.* 2004) was used as the calibration standard. Concordia diagrams and age calculations were performed using IsoPlot v. 3.70 (Ludwig 2001). BSE images of the analysed zircon grains (figures 3 and 5) were captured using a CAMECA SX100 Electron Probe Micro Analyser.

5. Results

5.1 *Samples from Karimnagar granulite belt*

EHV597 (Augen gneiss): A total of 54 zircons were recovered from the sample; these are euhedral to subhedral and are 150–250 µm in diameter (figure 3). Zircons are mostly unzoned with a few grains showing evidence of weak zonation (figure 3). Fourteen of the analyses are highly (>10%) discordant (table 3). These highly discordant data are rejected and are not used for the interpretation (table 3). The obtained U–Pb zircon age data form two concordant age groups. The dominant age group has a weighted average age of 1525±25 Ma (MSWD 25). The average Pb and U concentrations (table 3) are 148 (81–355 ppm) and 598 ppm (346–1398 ppm), respectively. The Th/U ratio (table 3) average is 0.8 (0.2–1.5). The second group (5 zircons) ranges in age between 873±13 and 1056±20 Ma and has a weighted average age of 953±79 Ma with MSWD of 18 (figure 4). The average Pb and U concentrations (table 3) are 20 (10–25 ppm) and 136 ppm (64–169 ppm), respectively. The Th/U ratio (table 3) average is 0.14 (0.1–0.3).

EHV592 (Banded gneiss): Zircons recovered are euhedral in shape and are 150–250 µm in diameter and are mostly unzoned (figure 3). A total of 42 zircons have been analysed. Unfortunately 19 grains produced highly discordant (>10% discordance)

results (table 4), which are rejected and not used in the interpretation. Analysis of this sample presents a single age group (figure 4) with an intercept age of 1621±36 Ma (MSWD 0.35). The average Pb and U concentrations (table 4) are 76 (47–138 ppm) and 299 ppm (184–509 ppm), respectively. The Th/U ratio (table 4) average is 1.1 (0.5–1.6).

EHV596 (Foliated granite): Zircon grains recovered from this sample are euhedral to subhedral, 150–250 µm in diameter and in some grains there is evidence of zoning (figure 3). A total of 69 zircon grains have been recovered and analysed (table 5), of which four analysis have suspicious U, Pb and Th concentrations, which have been removed (table 5), further removing of another 5 apparently inherited zircons, result in an intercept age of 2428±16 Ma (figure 4). This is interpreted as the intrusion age of the granite. The average Pb and U concentrations (table 5) are 49 (15–197 ppm) and 113 ppm (35–454 ppm), respectively. The Th/U ratio (table 5) average is 1.0 (0.5–2.4).

EHV593 (Schistose granite): Zircons are similar to those recovered from EHV596. A total of 30 grains have been analysed, of which 9 have high discordance and were removed (table 6). The U-Pb isotope system appears to be disturbed and did not result in an interpreted concordia age for this sample. Weighted average of the accepted single system ages (figure 4) result in 2480±31 Ma (MSWD 6.0). This is interpreted as the age of the granite with low confidence. The average Pb and U concentrations are 124 (45–522 ppm) and 288 ppm (106–1253 ppm), respectively. The Th/U ratio (table 6) average is 0.9 (0.2–2.0).

5.2 *Samples from Khammam schist belt*

EHV594 (Augen gneiss): Zircons recovered are euhedral to subhedral, are 150–250 µm in diameter and demonstrate some evidence of zoning (figure 5). A total of 43 zircon grains were recovered and analysed out of which 12 analyses are highly discordant (>10%; table 7) and are not used in the interpretation.

There are four different age groups evident from the data (figure 6 and table 7). Age group 1 is represented by two grains only with very concordant analyses. A weighted average age of 3212±36 Ma (MSWD 0.102) is obtained for the two grains. The average Pb and U concentrations (table 7) are 154 (151–158) and 258 ppm (244–271 ppm), respectively. The Th/U ratio (table 7) average is
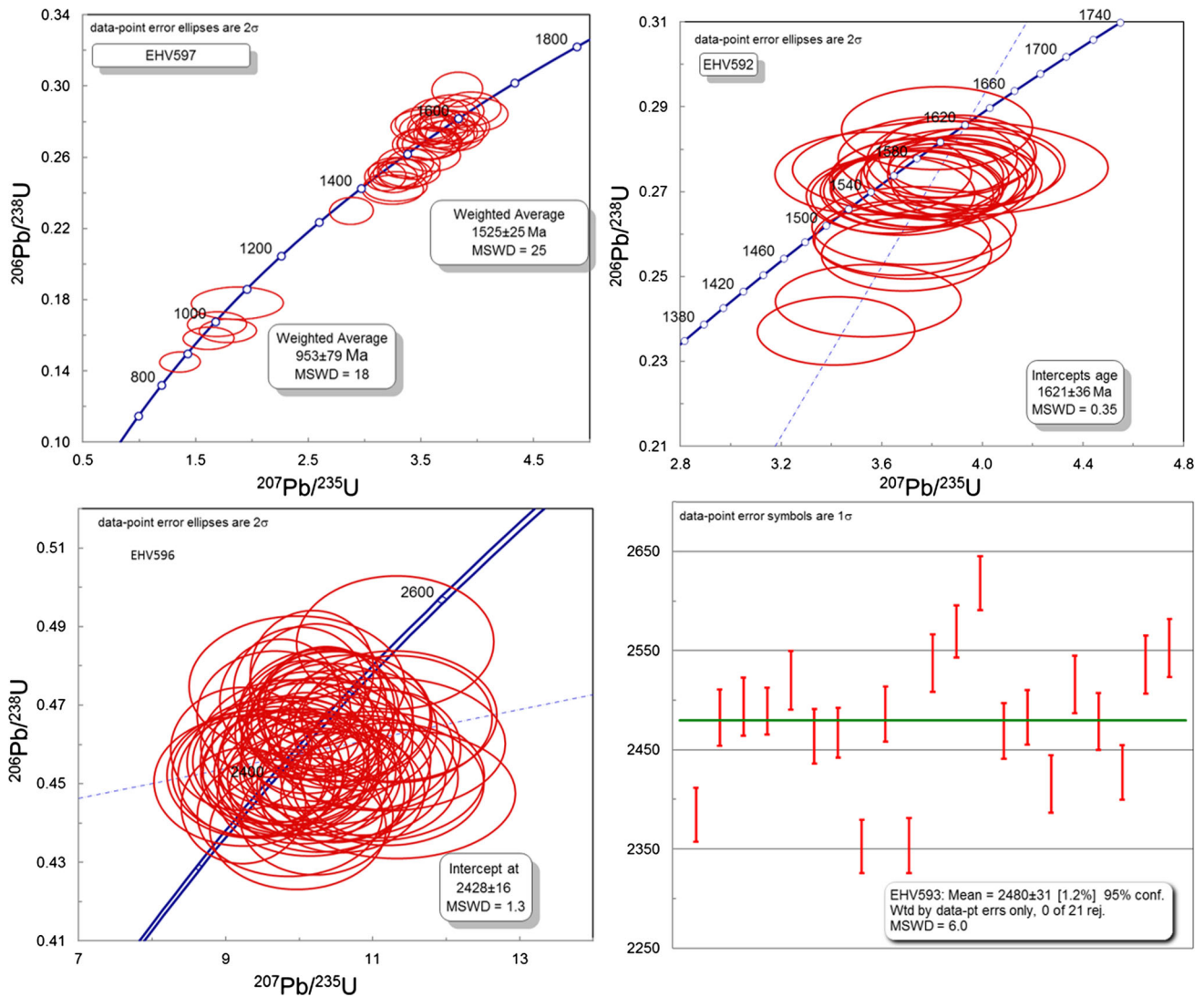
Figure 4. U–Pb concordia diagram of zircons from the Karimnagar granulites and the granites. EHV593 is the weighted average of accepted single system ages.

0.5 (0.4–0.5). Age group 2 has seven concordant data points and is represented with weighted average age of 2587±130 Ma (MSWD 23). The average Pb and U concentrations (table 7) for this group are 74 (44–103 ppm) and 164 ppm (81–217 ppm), respectively. The Th/U ratio (table 7) average is 0.9 (0.5–1.4). Age group 3 is the most prominent and is represented by 21 analyses of low discordance (<10%). This age group is represented with weighted average age of 1807±37 Ma (figure 6). The average Pb and U concentrations (table 7) for this group are 131 (32–405 ppm) and 454 ppm (115–1472 ppm), respectively with the Th/U ratio (table 7) average of 0.6 (0.2–1.9). The 4th group is represented by a single concordant zircon grain with an age of 522±25 Ma (figure 6 and table 7). The Pb and U concentrations for this zircon is 37

and 484 ppm, respectively with the Th/U ratio of 0.3 (table 7).

EHV591 (Quartzo-feldspathic gneiss): Zircons recovered are euhedral to subhedral and are 150–250 μm in diameter (figure 5). Zircons demonstrate stronger zonation than the samples from the KGB (figure 5). A total of 57 zircons were recovered and analysed, with eight analyses of high discordance (table 8 and figure 6). There are three different concordant age groups evident from the data (figure 6 and table 7).

Age group 1 is represented by three grains with <10% discordance and with a weighted average age of 3043±230 Ma. The average Pb and U concentrations (table 8) for this group are 50 (7–129 ppm) and 127 ppm (77–226 ppm), respectively with the Th/U ratio (table 8) average of 0.4 (0.4–0.5). Age

Table 4. *Results of U–Pb analysis of the zircons from sample EHV592 from the KGB.*

		Isotopic ratios				Age (Ma)					
	Grain-ID	$^{207}Pb/^{235}U$	2σ	$^{206}Pb/^{238}U$	2σ	$^{207}Pb/^{235}U$	1σ	$^{206}Pb/^{238}U$	1σ	$^{207}Pb/^{206}Pb$	1σ
1	EHV592-35	3.82002	0.31008	0.28497	0.00798	1597	32.66	1616.3	20	1574.6	49.39
2	EHV592-22	3.9005	0.25628	0.27891	0.00744	1613.8	26.55	1585.9	18.75	1575.9	41.55
3	EHV592-36	3.74888	0.29118	0.27318	0.00756	1581.9	31.13	1556.9	19.16	1580.2	48.41
4	EHV592-38	3.81626	0.3184	0.27808	0.00786	1596.2	33.56	1581.7	19.8	1621.2	50.52
5	EHV592-10	3.84041	0.24394	0.27766	0.00736	1601.3	25.59	1579.6	18.59	1619.4	39.19
6	EHV592-31	3.97763	0.2862	0.27593	0.0075	1629.6	29.19	1570.8	18.96	1626.4	44.86
7	EHV592-47	3.71841	0.2854	0.27035	0.0075	1575.3	30.71	1542.6	19.04	1597.3	50.67
8	EHV592-53	3.8727	0.51274	0.27544	0.00918	1608	53.42	1568.3	23.22	1626	71.8
9	EHV592-09	3.85965	0.26116	0.27351	0.00734	1605.3	27.28	1558.6	18.58	1636.3	40.53
10	EHV592-51	3.56618	0.31916	0.27432	0.00796	1542	35.49	1562.7	20.13	1641.3	55.8
11	EHV592-46	3.78511	0.31856	0.27097	0.00768	1589.6	33.8	1545.7	19.5	1625	52.76
12	EHV592-24	3.74311	0.2792	0.27073	0.00742	1580.6	29.88	1544.5	18.84	1624.1	45.01
13	EHV592-18	3.63525	0.27384	0.26924	0.0074	1557.3	29.99	1536.9	18.81	1621.2	44.62
14	EHV592-42	3.71752	0.29544	0.27035	0.00756	1575.1	31.79	1542.6	19.18	1633.5	50.21
15	EHV592-21	3.74324	0.27818	0.27346	0.0075	1580.7	29.77	1558.3	18.99	1650.9	44.34
16	EHV592-20	3.91868	0.24138	0.27447	0.00726	1617.5	24.92	1563.4	18.34	1657.8	39.29
17	EHV592-30	3.822	0.26552	0.27231	0.00736	1597.4	27.95	1552.5	18.66	1647.3	43.71
18	EHV592-52	3.68099	0.29654	0.26905	0.00758	1567.3	32.16	1536	19.23	1632.8	52.76
19	EHV592-32	3.85885	0.27918	0.27368	0.00746	1605.1	29.17	1559.5	18.9	1657.8	45.16
20	EHV592-43	3.67977	0.28806	0.25912	0.00722	1567	31.25	1485.3	18.47	1592.5	50.33
21	EHV592-45	3.91902	0.3188	0.27531	0.00776	1617.6	32.9	1567.7	19.59	1696.9	50.9
22	EHV592-26	3.72831	0.3314	0.26198	0.00752	1577.5	35.58	1500	19.2	1630.7	50.73
23	EHV592-01	3.93753	0.24478	0.2725	0.00722	1621.4	25.17	1553.5	18.28	1700.6	37.88
24	EHV592-33	3.72348	0.31894	0.25846	0.00736	1576.4	34.28	1482	18.87	1694.6	50.16
25	EHV592-41	3.54616	0.30134	0.24432	0.00696	1537.6	33.65	1409.1	18.02	1633.9	52.27
26	EHV592-44	3.69847	0.27608	0.25525	0.00706	1571	29.83	1465.5	18.11	1718.6	48.44
27	EHV592-48	3.41863	0.25564	0.23719	0.00658	1508.7	29.37	1372.1	17.14	1780.1	49.43
28	EHV592-07	3.96948	1.95404	0.19522	0.0191	1628	199.63	1149.6	51.53	2374.4	234.72
29	EHV592-39	4.11128	1.83606	0.17572	0.01576	1656.5	182.37	1043.5	43.23	2278.3	191.74
30	EHV592-14	3.10716	1.05606	0.15734	0.01136	1434.5	130.54	942	31.63	2087.5	166.89
31	EHV592-16	2.95478	0.82728	0.14788	0.00906	1396.1	106.2	889.1	25.43	2058.7	143.38
32	EHV592-13	2.63815	0.79724	0.14792	0.00994	1311.3	111.25	889.3	27.91	2070.8	160.22
33	EHV592-11	3.03606	0.9511	0.1632	0.01196	1416.7	119.64	974.5	33.13	2428.9	152.57
34	EHV592-23	3.55289	1.54968	0.16892	0.01676	1539.1	172.8	1006.2	46.19	2535.2	191.38
35	EHV592-29	3.71228	1.30538	0.16573	0.01302	1574	140.64	988.6	36	2535.9	159.89
36	EHV592-27	2.92568	0.95926	0.15134	0.01192	1388.6	124.06	908.5	33.34	2438.5	157.94
37	EHV592-04	3.98063	1.30612	0.1503	0.01064	1630.3	133.14	902.7	29.81	2431.9	145.17
38	EHV592-06	5.13352	1.6459	0.16677	0.01142	1841.7	136.24	994.3	31.53	2703.3	126.52
39	EHV592-40	3.55824	1.04662	0.14991	0.0104	1540.3	116.57	900.5	29.17	2558	132.6
40	EHV592-05	5.17333	1.23644	0.16527	0.00918	1848.2	101.68	986	25.4	2849.9	93.81
41	EHV592-08	4.79144	1.27696	0.16605	0.0104	1783.4	111.94	990.3	28.75	2871.6	108.38
42	EHV592-34	5.54612	3.24946	0.16857	0.02136	1907.8	252.02	1004.2	58.93	3228.8	199.08

Table 4. *(Continued.)*

	Disc (%)	Pb (ppm)	Th (ppm)	U (ppm)	Th/U	Accepted age (Ma)	1σ
1	−2.6	57.1	217.35	215.01	1.0	1616.3	20
2	−0.6	92.82	187.02	358.83	0.5	1585.9	18.75
3	1.5	62.85	280.87	246.79	1.1	1556.9	19.16
4	2.4	58.98	211.34	226.44	0.9	1581.7	19.8
5	2.5	130.65	732.72	509.89	1.4	1579.6	18.59
6	3.4	79.37	223.55	309.1	0.7	1570.8	18.96
7	3.4	89.76	288.2	353.4	0.8	1542.6	19.04
8	3.5	63.59	377.86	249.37	1.5	1568.3	23.22
9	4.7	71.31	248.32	282.65	0.9	1558.6	18.58
10	4.8	47.48	196.65	184.64	1.1	1562.7	20.13
11	4.9	70.8	214.54	275.19	0.8	1545.7	19.5
12	4.9	58.63	359.22	233.34	1.5	1544.5	18.84
13	5.2	59.18	171.13	235.07	0.7	1536.9	18.81
14	5.6	61.3	243.07	242.6	1.0	1542.6	19.18
15	5.6	61.46	314.02	242.44	1.3	1558.3	18.99
16	5.7	114.87	342.12	451.8	0.8	1563.4	18.34
17	5.8	95.32	307.12	376.45	0.8	1552.5	18.66
18	5.9	79.22	340.94	313.98	1.1	1536	19.23
19	5.9	75.81	470.83	297.56	1.6	1559.5	18.9
20	6.7	92.32	605.92	381.02	1.6	1485.3	18.47
21	7.6	72.06	337.81	279.73	1.2	1567.7	19.59
22	8.0	61.79	244.88	248.87	1.0	1500	19.2
23	8.6	92.33	395.11	368.18	1.1	1553.5	18.28
24	**12.5**	**84.83**	**259.55**	**339.01**	**0.8**	**NA**	**NA**
25	**13.8**	**111.96**	**804.59**	**458.45**	**1.8**	**NA**	**NA**
26	**14.7**	**88.75**	**453.23**	**371.74**	**1.2**	**NA**	**NA**
27	**22.9**	**99.41**	**455.19**	**450.24**	**1.0**	**NA**	**NA**
28	**51.6**	**1.326**	**18.96**	**7.37**	**2.6**	**NA**	**NA**
29	**54.2**	**1.282**	**10.27**	**7.63**	**1.3**	**NA**	**NA**
30	**54.9**	**1.588**	**9.96**	**10.84**	**0.9**	**NA**	**NA**
31	**56.8**	**1.78**	**12.02**	**12.37**	**1.0**	**NA**	**NA**
32	**57.1**	**1.69**	**12.53**	**12.33**	**1.0**	**NA**	**NA**
33	**59.9**	**1.72**	**17.76**	**11.42**	**1.6**	**NA**	**NA**
34	**60.3**	**0.708**	**1.81**	**4.52**	**0.4**	**NA**	**NA**
35	**61.0**	**1.274**	**13.31**	**8.27**	**1.6**	**NA**	**NA**
36	**62.7**	**1.427**	**15.51**	**10.15**	**1.5**	**NA**	**NA**
37	**62.9**	**1.499**	**10.7**	**10.84**	**1.0**	**NA**	**NA**
38	**63.2**	**1.98**	**30.06**	**12.91**	**2.3**	**NA**	**NA**
39	**64.8**	**1.41**	**8.47**	**10.17**	**0.8**	**NA**	**NA**
40	**65.4**	**147.69**	**8359.72**	**970.32**	**8.6**	**NA**	**NA**
41	**65.5**	**77.27**	**4763.23**	**504.64**	**9.4**	**NA**	**NA**
42	**68.9**	**0.555**	**8.28**	**3.53**	**2.3**	**NA**	**NA**

NA: Not Applicable. Bold data are rejected and not utilised in the analysis. Discordance is defined as $1 - (^{206}Pb/^{238}U \ Age \div {}^{207}Pb/^{206}Pb \ Age)$.

group 2 is most prominent with 45 data points, five of which are highly discordant (>10%) and are not used in the interpretation (table 8 and figure 6). This age group ranges between 2005±28 and 2541±29 Ma and with a weighted average age of 2396±24 Ma. The average Pb and U concentrations (table 8) for this group are 104 (6–441 ppm) and 279 (19–1034 ppm), respectively with the Th/U ratio (table 8) average of 1.2 (0.1–2.7). The third age group is represented by a single zircon grain giving an age of 472±9 Ma (figure 6 and table 8). The Pb and U concentrations for this zircon is 200 and 82 ppm, respectively with the Th/U ratio of 1.8 (table 8).

6. Discussion

Unravelling of overprinting multiple tectonothermal events by the *in-situ* U–Pb geochronology in

Table 5. *Results of U–Pb analysis of the zircons from granite sample EHV596 from the KGB.*

	Grain-ID	Isotopic ratios				Age (Ma)					
		$^{207}Pb/^{235}U$	2σ	$^{206}Pb/^{238}U$	2σ	$^{207}Pb/^{235}U$	1σ	$^{206}Pb/^{238}U$	1σ	$^{207}Pb/^{206}Pb$	1σ
1	EHV596-1	10.07794	0.71196	0.45813	0.01232	2442	32.63	2431.3	27.25	2456.5	31.55
2	EHV596-2	9.67685	0.63732	0.4548	0.01212	2404.5	30.31	2416.6	26.86	2458.6	30.79
3	EHV596-3	11.09264	0.87372	0.45133	0.01234	2530.9	36.68	2401.1	27.39	2523.1	32.5
4	EHV596-4	10.17783	1.11462	0.45997	0.137	2451.1	50.63	2439.4	30.24	2465.6	39.77
5	EHV596-5	10.35283	0.68404	0.46964	0.01248	2466.8	30.59	2482	27.9	2475.8	30.6
6	EHV596-6	10.58187	0.91666	0.44782	0.01254	2487.1	40.18	2385.6	29.42	2556.6	34.29
7	EHV596-7	10.49763	1.0556	0.45607	0.01328	2479.7	46.61	2422.2	29.79	2566.9	37.29
8	EHV596-8	11.27548	1.1557	0.46723	0.01356	2546.2	47.8	2471.4	27.23	2536.4	37.24
9	EHV596-9	10.07898	0.65594	0.46625	0.01238	2442	30.06	2467.1	28.65	2519.9	30.54
10	EHV596-10	13.39071	1.01318	0.49041	0.01324	2707.6	35.74	2572.4	30.05	2715.5	30.83
11	EHV596-11	11.30649	1.09636	0.48596	0.01386	2548.7	45.23	2553.2	29.15	2495.8	36.3
12	EHV596-12	10.07882	1.00954	0.45305	0.01314	2442	46.26	2408.8	29.87	2478.5	38.04
13	EHV596-13	11.00624	1.23544	0.45192	0.01346	2523.7	52.24	2403.8	27.89	2506.9	39.84
14	EHV596-14	10.21709	0.73002	0.47508	0.01276	2454.6	33.04	2505.8	27.55	2472.1	32.12
15	EHV596-15	11.15913	0.84782	0.45861	0.01246	2536.5	35.4	2433.4	29.64	2645.9	32.17
16	**EHV596-16**	**10.38326**	**1.08878**	**0.45884**	**0.01342**	**2469.6**	**48.56**	**2434.4**	**29.64**	**2442.4**	**41.15**
17	EHV596-17	9.96804	1.1988	0.47496	0.0145	2431.8	55.49	2505.3	31.68	2357	43.56
18	EHV596-18	10.9153	0.96326	0.45897	0.01278	2515.9	41.04	2435	28.25	2481.4	35.28
19	EHV596-19	9.88702	0.81224	0.4557	0.01258	2424.3	37.88	2420.5	27.87	2483.9	34.7
20	EHV596-20	10.47782	1.06632	0.4671	0.01352	2478	47.17	2470.8	29.7	2447.7	38.62
21	EHV596-21	9.86979	0.98804	0.46011	0.01336	2422.7	46.15	2440	29.47	2471.5	38.81
22	EHV596-22	10.40256	1.12682	0.45164	0.01328	2471.3	50.17	2402.5	29.5	2427.2	40.39
23	EHV596-23	9.35649	0.82162	0.45211	0.01268	2373.6	40.28	2404.6	28.13	2408.2	36.87
24	EHV596-24	9.98316	0.98036	0.43857	0.01264	2433.2	45.32	2344.3	28.34	2507	38.45
25	EHV596-25	9.8082	0.93628	0.45262	0.01294	2416.9	43.98	2406.9	28.7	2445.9	38.28
26	EHV596-26	13.48328	1.3981	0.4669	0.01358	2714.1	49.01	2469.9	29.84	2832	36.59
27	EHV596-27	9.5752	0.90008	0.45567	0.01296	2394.8	43.21	2420.4	28.7	2400.5	38.44
28	EHV596-28	10.3123	0.89966	0.46128	0.01288	2463.2	40.38	2445.2	28.39	2499.2	36.36
29	EHV596-30	12.51286	1.80358	0.48706	0.01574	2643.7	67.76	2557.9	34.11	2574.6	46.29
30	EHV596-31	10.48764	0.6521	0.4641	0.01216	2478.8	28.82	2457.6	26.79	2471.3	32.38
31	EHV596-32	10.28483	1.00744	0.44836	0.01286	2460.7	45.32	2388	28.61	2477.5	39.15
32	EHV596-33	10.39583	0.78382	0.4684	0.01266	2470.7	34.92	2476.5	27.77	2456.3	34.93
33	EHV596-34	11.19542	1.3146	0.46003	0.01384	2539.5	54.73	2439.7	30.54	2490.7	42.7
34	**EHV596-35**	**10.25522**	**1.1**	**0.44725**	**0.0132**	**2458.1**	**49.62**	**2383**	**29.4**	**2505.4**	**41.41**

35	EHV596-36	10.1253	0.95162	0.45978	2446.3	43.43	2438.6	0.01304	28.79	2441.2	39.06
36	EHV596-37	9.88794	0.97768	0.45312	2424.4	45.59	2409.1	0.01302	28.86	2406.3	40.4
37	EHV596-38	10.23523	0.85028	0.44168	2456.3	38.42	2358.1	0.01216	27.21	2479.8	37.01
38	EHV596-39	9.21323	0.78612	0.4589	2359.4	39.08	2434.7	0.01278	28.23	2399	38.39
39	EHV596-40	9.81877	1.03536	0.45592	2417.9	48.59	2421.5	0.01338	29.61	2420.6	42.27
40	EHV596-41	10.42605	0.925	0.46474	2473.4	41.1	2460.4	0.01298	28.58	2474.6	38.56
41	EHV596-42	10.89921	0.79676	0.4635	2514.6	33.99	2455	0.01244	27.4	2499.2	35.75
42	EHV596-43	10.8714	0.91742	0.45214	2512.2	39.23	2404.7	0.01244	27.61	2442.7	37.99
43	EHV596-44	9.89072	1.0095	0.45558	2424.6	47.06	2420	0.01326	29.34	2448.3	42.09
44	EHV596-45	10.11902	0.80872	0.46305	2445.7	36.93	2453	0.01268	27.92	2471.3	37.74
45	EHV596-46	9.43361	0.94964	0.45265	2381.1	46.21	2407	0.01316	29.18	2423.6	42.49
46	**EHV596-47**	**11.53651**	**1.1432**	**0.45004**	**2567.5**	**46.3**	**2395.4**	**0.013**	**28.89**	**2703.6**	**40.06**
47	EHV596-48	10.05135	0.94122	0.45032	2439.5	43.24	2396.7	0.01274	28.31	2399.9	41.05
48	EHV596-49	9.40295	0.9825	0.45244	2378.1	47.95	2406.1	0.0133	29.53	2431.8	43.73
49	EHV596-50	9.87239	1.02886	0.44229	2422.9	48.04	2360.9	0.01296	28.96	2470.4	43.31
50	EHV596-51	10.3611	0.96864	0.46814	2467.6	43.29	2475.4	0.01322	29.01	2384.7	41.56
51	EHV596-52	10.00468	0.73158	0.47428	2435.2	33.75	2502.3	0.01276	27.89	2401.2	38.29
52	**EHV596-53**	**14.08361**	**1.68042**	**0.50205**	**2755.4**	**56.56**	**2622.6**	**0.01522**	**32.65**	**2808.1**	**43.01**
53	EHV596-54	9.24223	0.69188	0.44442	2362.3	34.3	2370.4	0.01204	26.86	2405.4	39.16
54	EHV596-55	9.25857	1.00898	0.45072	2363.9	49.93	2398.4	0.01352	30.03	2480.7	45.69
55	EHV596-56	11.20985	1.0649	0.44993	2540.7	44.28	2395	0.01276	28.35	2512.3	41.82
56	EHV596-57	9.73763	0.66768	0.47143	2410.3	31.57	2489.8	0.01258	27.54	2423.5	38.52
57	EHV596-58	10.17282	0.6847	0.47856	2450.6	31.11	2521	0.0127	27.7	2390.5	38.59
58	EHV596-59	10.49621	0.87546	0.45027	2479.6	38.66	2396.5	0.01242	27.62	2490.4	40.81
59	EHV596-60	10.05824	0.70874	0.45348	2440.1	32.54	2410.7	0.01214	26.93	2443.3	39.29
60	EHV596-61	10.15977	1.04148	0.44751	2449.4	47.38	2384.2	0.01298	28.91	2403.1	45.23
61	EHV596-62	12.86153	1.10458	0.48761	2669.6	40.46	2560.3	0.01352	29.29	2677	40.65
62	EHV596-63	11.34639	1.3038	0.44737	2552	53.61	2383.6	0.0134	29.83	2515.8	46.7
63	EHV596-64	11.32915	1.05862	0.46645	2550.6	43.59	2468	0.0132	29.01	2523.7	43.2
64	EHV596-65	10.3659	0.76006	0.46903	2468	33.95	2479.3	0.01264	27.74	2411.4	41.05
65	EHV596-66	10.17769	0.67806	0.46606	2451.1	30.8	2466.3	0.01238	27.23	2413.9	40.34
66	EHV596-67	9.65598	0.85474	0.46772	2402.5	40.72	2473.5	0.01314	28.84	2385.1	44.2
67	EHV596-68	10.65726	0.9381	0.46669	2493.7	40.86	2469	0.0131	28.77	2545.6	43.32
68	EHV596-69	12.41924	1.4659	0.46427	2636.6	55.46	2458.4	0.01408	31	2672	47.15
69	EHV596-70	10.36654	0.82838	0.45208	2468.1	37	2404.5	0.0124	27.54	2473.9	42.85

Table 5. *(Continued.)*

	Disc (%)	Pb (ppm)	Th (ppm)	U (ppm)	Th/U	Accepted age (Ma)	1σ
1	1.0	58.29	121.39	136.22	0.9	2431.3	27.25
2	1.7	68.07	158.84	160.24	1.0	2416.6	26.86
3	4.8	43.62	78.24	103.48	0.8	2401.1	27.39
4	1.1	32.4	75.62	75.41	1.0	2439.4	30.24
5	−0.3	65.54	131.4	149.43	0.9	2482	27.39
6	6.7	34.09	94.25	81.52	1.2	2385.6	27.9
7	5.6	22.45	38.76	52.71	0.7	2422.2	29.42
8	2.6	22.9	59.89	52.49	1.1	2471.4	29.79
9	2.1	71.46	102.98	164.16	0.6	2467.1	27.23
10	5.3	83.96	178.39	183.38	1.0	2572.4	28.65
11	−2.3	56.14	136.84	123.76	1.1	2553.2	30.05
12	2.8	23.54	48.48	55.66	0.9	2408.8	29.15
13	4.1	17.71	35.38	43.53	0.8	2403.8	29.87
14	−1.4	34.72	38.6	80.9	0.5	2505.8	27.89
15	8.0	51.89	291.88	121.23	2.4	2433.4	27.55
16	**0.3**	**1.56**	**NA**	**1.03**	**NA**	**2434.4**	**29.64**
17	−6.3	15.57	31.66	35.23	0.9	2505.3	31.68
18	1.9	37.8	92.33	88.28	1.0	2435	28.25
19	2.6	37.53	93.6	88.27	1.1	2420.5	27.87
20	−0.9	33.79	42.77	77.53	0.6	2470.8	29.7
21	1.3	25.84	67.88	60.2	1.1	2440	29.47
22	1.0	21.24	33.12	50.41	0.7	2402.5	29.5
23	0.1	33.34	80.11	79.06	1.0	2404.6	28.13
24	6.5	24.61	44.41	60.16	0.7	2344.3	28.34
25	1.6	25.94	50.95	61.45	0.8	2406.9	28.7
26	12.8	19.75	44.89	45.09	1.0	NA	NA
27	−0.8	29.4	66.09	69.19	1.0	2420.4	28.7
28	2.2	35.16	80.18	81.75	1.0	2445.2	28.39
29	0.6	23.82	42.13	52.46	0.8	2557.9	34.11
30	0.6	114.09	281.96	263.72	1.1	2457.6	26.79
31	3.6	27.6	52.53	66.05	0.8	2388	28.61
32	−0.8	85.78	289.97	196.51	1.5	2476.5	27.77
33	2.0	16.38	37.42	36.58	1.0	2439.7	30.54
34	**4.9**	**NA**	**NA**	**NA**	**NA**	**2383**	**29.4**
35	0.1	31.62	77.05	73.81	1.0	2438.6	28.79
36	−0.1	27.39	60.36	64.88	0.9	2409.1	28.86
37	4.9	42.12	76.67	102.35	0.7	2358.1	27.21
38	−1.5	40.64	144.45	95.05	1.5	2434.7	28.23
39	0.0	23.33	57.02	54.94	1.0	2421.5	29.61
40	0.6	44.7	73.87	103.28	0.7	2460.4	28.58
41	1.8	73.81	163.21	170.98	1.0	2455	27.4
42	1.6	51.39	141.41	122.05	1.2	2404.7	27.61
43	1.2	28.16	82.3	66.38	1.2	2420	29.34
44	0.7	53.86	93.98	124.93	0.8	2453	27.92
45	0.7	26.57	69.13	63.05	1.1	2407	29.18
46	**11.4**	**49.91**	**98.73**	**119.12**	**0.8**	**NA**	**NA**
47	0.1	33.57	156.5	80.09	2.0	2396.7	28.31
48	1.1	23.26	50.97	55.24	0.9	2406.1	29.53
49	4.4	26.44	108.33	64.23	1.7	2360.9	28.96
50	−3.8	38.87	62.48	89.22	0.7	2475.4	29.01
51	−4.2	81.56	171.85	184.8	0.9	2502.3	27.89
52	**6.6**	**NA**	**NA**	**0.84**	**NA**	**2622.6**	**32.65**

Table 5. *(Continued.)*

	Disc (%)	Pb (ppm)	Th (ppm)	U (ppm)	Th/U	Accepted age (Ma)	1σ
53	1.5	70.05	147.58	169.43	0.9	2370.4	26.86
54	3.3	18.63	70.99	40.72	1.7	2398.4	30.03
55	4.7	33.96	85.05	81.13	1.0	2395	28.35
56	−2.7	113.04	318.76	257.81	1.2	2489.8	27.54
57	−5.5	132.3	210.98	297.26	0.7	2521	27.7
58	3.8	48.53	141.06	115.89	1.2	2396.5	27.62
59	1.3	105.52	255.92	250.24	1.0	2410.7	26.93
60	0.8	30.37	91.22	72.99	1.2	2384.2	28.91
61	4.4	55.82	117.92	123.13	1.0	2560.3	29.29
62	5.3	23.43	55.42	56.34	1.0	2383.6	29.83
63	2.2	53.55	114.77	123.5	0.9	2468	29.01
64	−2.8	125.02	375.46	286.81	1.3	2479.3	27.74
65	−2.2	196.87	612.01	454.54	1.3	2466.3	27.23
66	−3.7	47.66	94.31	109.67	0.9	2473.5	28.84
67	3.0	49.03	65.94	113.08	0.6	2469	28.77
68	8.0	20.3	47.05	41.72	1.1	2458.4	31
69	2.8	123.13	360.46	293.18	1.2	2404.5	27.54

NA: Not applicable. Bold data are rejected and not utilised in the analysis. Discordance is defined as $1 - ({}^{206}Pb/{}^{238}U$ Age $\div {}^{207}Pb/{}^{206}Pb$ Age).

single samples have been reported earlier (Wang *et al.* 2007; Zhang *et al.* 2008; Ma *et al.* 2012), based on resetting of the U–Pb system in pre-existing zircons due to tectonothermal effects or multiple recrystallization of new zircons during metamorphism (Carson *et al.* 2002). The zircons grown under metamorphic conditions have lower Th/U, typically lower than 0.1, whereas the magmatic zircons have higher Th/U ratios 0.18–0.47 (Rubatto 2002). However, Wang *et al.* (2011) demonstrate a huge variation in the Th/U in the granitic rocks (0.1–3.79) and in the intermediate rocks (0.02–6.82). Zircon growth with high Th/U ratios (>1) has also been reported during UHT metamorphism (Carson *et al.* 2002). The Th/U ratio for the gneissic samples from the KGB and the KSB show high values (0.14–1.8) on average (tables 3–8). We interpret the concordant ages obtained from the KGB and KSB to be representing relict magmatic zircons (representing either original igneous protolith or detrital), which has the U–Pb system reset by the tectonothermal events.

The NKSB, EGMB, KGB are important pieces in the reconstruction of the Proterozoic history of the Indian continent and its part in the global tectonic framework and supercontinent cycle (Meert 2012; Nance *et al.* 2013; Meert *et al.* 2017). The results presented in this contribution demonstrate that the samples of KGB and northern NKSB are unique in terms of their zircon U–Pb geochronology

suggesting a distinct, tectonothermal history relative to each other (figure 7). The different rock samples were collected from localities currently in close proximity (within ∼50 km of one another) from the eastern part of KGB and the northern Khammam schist belt of the NKSB.

The granite samples from the KGB are ∼2400 Ma old (intercept age of EHV596 is 2428±16 Ma and the schistose granite sample (EHV593) show a weighted average age of 2480±31 Ma). The interpreted age of 2400–2500 Ma for the granite within the KGB is in good agreement with the previously reported Rb–Sr whole rock age result of 2490± 115 Ma (Crawford 1969). This Late Archaean event is also reported as a metamorphic imprint in the zircons of granulites from KGB by Santosh *et al.* (2004). However, Rajesham *et al.* (1993) consider the 2.5 Ga event to represent peak metamorphism of the KGB rocks to granulite grade. Recently, Prakash *et al.* (2017) date this peak metamorphism earlier than the granite event at 2604±25 Ma.

The two samples of gneisses (EHV597 and EHV592) from the KGB were collected from the same area and combined constitute a prominent 1560–1600 Ma age group. The 1000 Ma old event recorded in EHV597 is not evident from the concordant ages in EHV592 (figure 4). Combining the results from all four samples, the KGB is interpreted to record metamorphic resetting at

Table 6. *Results of U-Pb analysis of the zircons from granite sample EHV593 from the KGB.*

	Grain-ID	Isotopic ratios				Ages (Ma)					
		207Pb/235U	2σ	206Pb/238U	2σ	207Pb/235U	1σ	206Pb/238U	1σ	207Pb/206Pb	1σ
1	EHV593-01	10.166	0.348	0.448	0.006	2450.0	31.6	2384.5	27.4	2588.5	30.6
2	EHV593-02	11.856	0.408	0.470	0.006	2593.1	32.2	2482.6	28.3	2731.7	29.8
3	**EHV593-06**	**12.098**	**0.287**	**0.426**	**0.006**	**2612.0**	**22.2**	**2289.0**	**25.3**	**2903.5**	**26.3**
4	EHV593-09	10.948	0.461	0.472	0.007	2518.7	39.2	2493.2	29.3	2512.3	34.1
5	EHV593-10	10.603	0.268	0.444	0.006	2489.0	23.5	2366.6	26.1	2587.4	27.9
6	EHV593-14	10.532	0.439	0.478	0.007	2482.7	38.7	2520.2	29.5	2491.1	34.7
7	EHV593-15	11.473	0.362	0.465	0.006	2562.4	29.5	2463.6	27.6	2591.3	30.4
8	**EHV593-16**	**12.817**	**0.382**	**0.467**	**0.006**	**2666.3**	**28.1**	**2471.3**	**27.5**	**2887.1**	**29.0**
9	EHV593-17	10.356	0.280	0.472	0.006	2467.1	25.0	2494.4	27.4	2540.4	29.6
10	EHV593-19	10.026	0.327	0.440	0.006	2437.2	30.2	2352.5	26.7	2505.4	32.0
11	**EHV593-20**	**11.346**	**0.276**	**0.443**	**0.006**	**2552.0**	**22.7**	**2362.5**	**26.0**	**2692.1**	**28.8**
12	EHV593-21	11.408	0.344	0.471	0.006	2557.1	28.2	2486.1	27.6	2588.8	31.0
13	EHV593-23	10.965	0.444	0.441	0.006	2520.1	37.7	2353.6	27.7	2630.1	34.9
14	**EHV593-24**	**11.591**	**0.448**	**0.430**	**0.006**	**2572.0**	**36.1**	**2305.0**	**27.0**	**2731.3**	**33.9**
15	EHV593-28	11.354	0.427	0.482	0.007	2552.6	35.1	2537.3	29.0	2516.9	34.9
16	EHV593-29	11.560	0.324	0.477	0.006	2569.4	26.2	2514.7	27.7	2598.0	31.9
17	EHV593-30	12.175	0.352	0.467	0.006	2618.0	27.2	2469.0	27.4	2711.0	32.0
18	EHV593-31	11.770	0.441	0.467	0.006	2586.3	35.1	2469.0	28.3	2586.1	35.3
19	EHV593-32	12.473	0.382	0.470	0.006	2640.7	28.8	2482.8	27.7	2744.2	33.0
20	EHV593-33	10.946	0.491	0.455	0.007	2518.6	41.7	2415.4	28.9	2526.1	38.9
21	**EHV593-36**	**11.839**	**0.382**	**0.422**	**0.006**	**2591.8**	**30.2**	**2267.6**	**25.9**	**2843.9**	**34.1**
22	**EHV593-38**	**13.031**	**0.413**	**0.444**	**0.006**	**2681.9**	**29.9**	**2370.1**	**26.8**	**2915.6**	**34.1**
23	EHV593-39	11.864	0.465	0.477	0.007	2593.7	36.7	2516.1	29.0	2611.7	37.6
24	EHV593-42	10.807	0.420	0.469	0.007	2506.7	36.1	2478.3	28.7	2524.0	39.1
25	EHV593-43	11.724	0.386	0.457	0.006	2582.6	30.8	2427.3	27.5	2670.8	36.9
26	**EHV593-46**	**12.509**	**0.381**	**0.421**	**0.006**	**2643.4**	**28.6**	**2265.8**	**25.7**	**2923.6**	**36.2**
27	EHV593-47	12.609	0.472	0.482	0.007	2650.9	35.2	2535.9	29.0	2727.9	38.8
28	**EHV593-48**	**10.835**	**0.493**	**0.433**	**0.006**	**2509.0**	**42.3**	**2318.1**	**28.2**	**2640.7**	**42.4**
29	EHV593-50	12.955	0.491	0.486	0.007	2676.4	35.8	2552.8	29.3	2727.9	39.8
30	**EHV593-51**	**12.107**	**0.392**	**0.454**	**0.006**	**2612.7**	**30.4**	**2414.7**	**27.4**	**2765.5**	**38.9**

Table 6. *(Continued.)*

	Disc (%)	Pb (ppm)	Th (ppm)	U (ppm)	Th/U	Accepted age (Ma)	1σ
1	7.9	90.87	195.91	204.7	1.0	2384.5	27.38
2	9.1	63.38	114.81	143.21	0.8	2482.6	28.26
3	**21.2**	**317.17**	**199.27**	**791.13**	**0.3**	**NA**	**NA**
4	0.8	48.68	97.62	109.76	0.9	2493.2	29.27
5	8.5	522.28	707.7	1253.96	0.6	2489	23.49
6	−1.2	55.26	109.32	123.24	0.9	2520.2	29.49
7	4.9	96.67	132.98	221.67	0.6	2463.6	27.59
8	**14.4**	**117.23**	**167.32**	**267.89**	**0.6**	**NA**	**NA**
9	1.8	181.57	73.3	453.02	0.2	2467.1	25.04
10	6.1	87.43	226.87	212.16	1.1	2352.5	26.73
11	**12.2**	**378.8**	**90.61**	**914.89**	**0.1**	**NA**	**NA**
12	4.0	151.35	131.88	344.05	0.4	2486.1	27.63
13	10.5	49.74	96.45	120.83	0.8	2353.6	27.74
14	**15.6**	**57.47**	**120.88**	**143.15**	**0.8**	**NA**	**NA**
15	−0.8	69.04	155.25	153.44	1.0	2537.3	28.96
16	3.2	220.26	224.4	495	0.5	2569.4	26.19
17	8.9	208.71	559.82	479.64	1.2	2618	27.15
18	4.5	70.55	319.66	162.22	2.0	2469	28.31
19	9.5	168.48	217.15	384.89	0.6	2482.8	27.67
20	4.4	44.95	91.89	106.17	0.9	2415.4	28.85
21	**20.3**	**126.73**	**115.28**	**322.98**	**0.4**	**NA**	**NA**
22	**18.7**	**275.75**	**410.31**	**667.02**	**0.6**	**NA**	**NA**
23	3.7	70.03	177.9	157.7	1.1	2516.1	29.02
24	1.8	71.18	286.19	163.37	1.8	2478.3	28.68
25	9.1	158.12	258.53	372.21	0.7	2427.3	27.47
26	**22.5**	**273.73**	**230.1**	**699.9**	**0.3**	**NA**	**NA**
27	7.0	85.92	127.79	192.02	0.7	2535.9	29.04
28	**12.2**	**40.94**	**108.75**	**101.93**	**1.1**	**NA**	**NA**
29	6.4	90.93	135.15	201.68	0.7	2552.8	29.27
30	**12.7**	**249.43**	**250.61**	**591.79**	**0.4**	**NA**	**NA**

NA: Not applicable. Bold data are rejected and not utilised in the analysis.
Discordance is defined as $1 - (^{206}\text{Pb}/^{238}\text{U Age} \div ^{207}\text{Pb}/^{206}\text{Pb Age})$.

∼1600 Ma with a later tectonothermal event at ∼1000 Ma. The granite intrusions at 2400–2500 Ma most likely form part of the regional Late Archaean granite magmatism within the Dharwar craton (Jayananda *et al.* 2013). The 3100 and 2600 Ma ages reported by Santosh *et al.* (2004) for the western KGB could not be reproduced in our samples. This suggests that the 1600 Ma event was intense enough to reset the U–Pb system in the zircons completely. However, we report a 1000 Ma Grenvillian tectonothermal event in the KGB, which was hitherto unreported.

Santosh *et al.* (2004), based on the absence of the Mesoproterozoic tectonothermal event in the KGB and the prominence of the 1600 Ma event in the BGB, proposed that the KGB and BGB evolved under different P–T conditions at different times. We report an intense 1600 Ma event from the southeastern part of the KGB and propose that the two granulite belts are probably affected by the same tectonic event. The 1600 Ma event marks the fragmentation of the craton and the development of the P–G valley (Chaudhuri *et al.* 2012). The ∼1600 Ma event was also identified in detrital zircon populations from the Sullavai Group of the P–G rift (Joy *et al.* 2015). We note that Basu and Bickford (2015) consider the glauconite ages reported from the Somanpalli Group and Pandikunta Limestone to be unreliable (cf., Conrad *et al.* 2011). They consider the deposition of Somanpalli rocks to have started after the eastern Dharwar–Bastar amalgamation at ∼1600 Ma, with deformation being due to the continued crustal shortening that followed craton amalgamation.
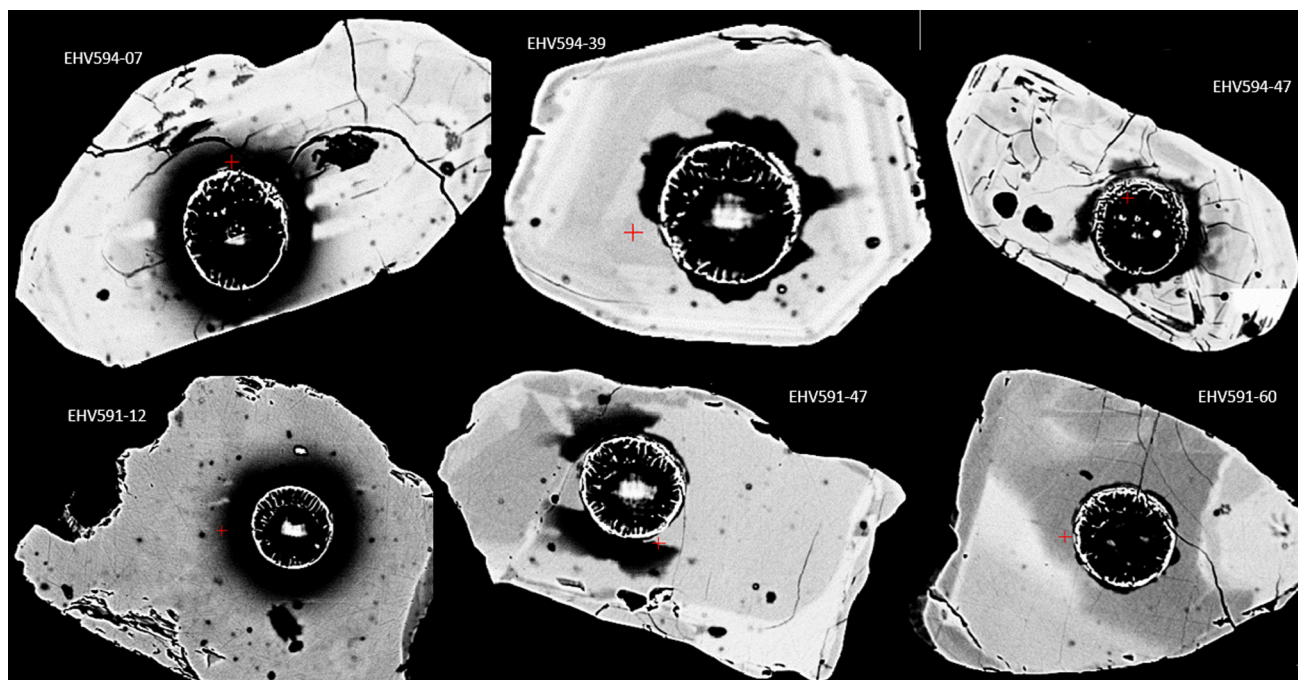
Figure 5. Examples of back scatter electron Z images captured using a CAMECA SX100 Electron Probe Micro Analyser for samples from the Khammam schist belt. Ablation spots are 35 µm in diameter and can be seen as circular holes.

The present report of a 1000 Ma tectonothermal event from the gneissic rocks of the KGB is contrary to Santosh *et al.* (2004). The presence of this Grenvillian age in the KGB, which is very prominent in the EGMB, highlights that both the KGB and EGMB were part of the global Grenvillian orogenic belt during the Rodinia supercontinent formation (figure 7). Unfortunately, the age of reassembly of the Dharwar and Bastar cratons cannot be constrained. Based on geological and structural analysis, it was suggested that suturing occurred subsequently to Mulug Group deposition (1565 Ma), but prior to Albaka and Sullavai Group deposition (Chaudhuri *et al.* 2012). The age of the Sullavai Group has recently been shown to be younger than 710 Ma (Joy *et al.* 2015). The 1000 Ma event reported herein is thus best interpreted as the age of 'Grenvillian' orogeny by which the Dharwar and Bastar cratons were reassembled.

It has been previously demonstrated that the NKSB records multiple deformation and metamorphism cycles, as well as granitic and alkaline intrusive magmatism (Saha *et al.* 2015 and references therein). Our NKSB samples represent unique and contrasting geochronological signatures to the samples from the KGB including the granite. The samples EHV594 and EHV591 show presence of Archaean zircons. The 3100–3250 Ma ages, which are interpreted as relict zircons (either representing protolith or detrital zircons as the nature of the protolith of the gneisses sampled, whether igneous or sedimentary has not been established during this study) of the Khammam schist belt of the NKSB (figures 6 and 7).

For sample EHV594, the prominent age range is ∼1800 Ma. This age range is not very apparent in EHV591, where 2400 Ma age is most prominent. Sample EHV594 also shows the 2400–2700 Ma age range, though not as pronounced as recorded in EHV591 (figure 6). The 1900 Ma age has also been reported previously in the Sm–Nd isochron age of the gabbro intrusions (Vadlamani 2010) and the $^{207}Pb/^{206}Pb$ zircon evaporation ages of andesitic rocks (Vadlamani *et al.* 2012) in the Vinjamuru Group, and the U–Pb xenotime age from the Udaigiri Group (Das *et al.* 2015). The KOC with an age range of 1850–1900 Ma (Vadlamani 2010; Vijaya Kumar *et al.* 2010) is postulated to represent orogenic accretion that led to Columbia supercontinent assembly (Saha *et al.* 2015).

Both EHV591 and EHV594 record a ca. 500 Ma age from a few zircon grains. The 500 Ma event is also recorded in the amphibolites from the Khammam schist belt (Okudaira *et al.* 2001), the mylonites of the Vinikonda Granite

Table 7. *Results of U–Pb analysis of the zircons from sample EHV594 from the Khammam belt of NKSB.*

		Isotopic ratios				Age (Ma)					
	Grain-ID	$^{207}Pb/^{235}U$	2σ	$^{206}Pb/^{238}U$	2σ	$^{207}Pb/^{235}U$	1σ	$^{206}Pb/^{238}U$	1σ	$^{207}Pb/^{206}Pb$	1σ
1	EHV594-11	0.63798	0.0391	0.08438	0.00232	501.1	12.12	522.2	6.92	476.7	55.08
2	EHV594-44	3.94712	0.23554	0.27705	0.0074	1623.4	24.17	1576.5	18.7	1617.2	40.89
3	EHV594-32	4.45232	0.24496	0.2992	0.00794	1722.1	22.81	1687.3	19.69	1704.9	36.38
4	EHV594-46	4.87807	0.47	0.30036	0.00888	1798.5	40.59	1693.1	22.03	1825.6	51.04
5	EHV594-38	4.94522	0.31122	0.30491	0.00824	1810	26.58	1715.6	20.34	1923.9	38.51
6	EHV594-40	4.48086	0.25484	0.30599	0.00814	1727.4	23.61	1720.9	20.07	1724.2	38.3
7	EHV594-51	4.62017	0.35958	0.30614	0.00858	1752.9	32.48	1721.7	21.18	1807	46.67
8	EHV594-09	5.10884	0.27568	0.3132	0.00838	1837.6	22.91	1756.4	20.56	1902.7	31.69
9	EHV594-24	5.50898	0.42682	0.31532	0.00884	1902	33.29	1766.8	21.68	1919.8	39.99
10	EHV594-19	5.1409	0.35154	0.31579	0.0087	1842.9	29.06	1769.2	21.29	1887.2	37.05
11	EHV594-13	5.36428	0.37828	0.32519	0.00902	1879.2	30.18	1815	21.93	1921.7	36.79
12	EHV594-45	5.29008	0.35432	0.3289	0.00894	1867.3	28.6	1833	21.69	1896.7	41.17
13	EHV594-33	5.07212	0.33454	0.3318	0.00902	1831.5	27.97	1847.1	21.83	1813.8	38.88
14	EHV594-48	5.04147	0.43302	0.33188	0.0095	1826.3	36.39	1847.5	22.98	1797.4	47.95
15	EHV594-43	5.45306	0.3291	0.33289	0.0089	1893.2	25.89	1852.4	21.54	1909.3	38.91
16	EHV594-23	5.21335	0.34476	0.3342	0.00912	1854.8	28.17	1858.7	22.04	1871.8	36.92
17	EHV594-28	5.19656	0.4007	0.33924	0.00952	1852.1	32.83	1883	22.9	1859.5	41.03
18	EHV594-39	5.29038	0.31496	0.34122	0.00912	1867.3	25.42	1892.5	21.92	1861	37.91
19	EHV594-49	5.48719	0.42486	0.3438	0.00958	1898.6	33.25	1904.9	22.99	1848.8	44.96
20	EHV594-26	5.2862	0.35078	0.34451	0.0094	1866.6	28.33	1908.3	22.55	1898.6	37.21
21	EHV594-20	5.40977	0.33074	0.34518	0.00932	1886.4	26.2	1911.5	22.31	1853.2	34.86
22	EHV594-27	5.5085	0.4633	0.34727	0.0099	1901.9	36.14	1921.5	23.69	1853.6	42.73
23	EHV594-30	11.02407	0.92012	0.44821	0.01262	2525.2	38.85	2387.3	28.09	2563	35.95
24	EHV594-14	10.52545	0.71698	0.46364	0.01266	2482.2	31.58	2455.6	27.88	2490.1	31.12
25	EHV594-47	11.38573	1.00092	0.48787	0.01388	2555.3	41.03	2561.5	30.07	2587.1	40.43
26	EHV594-16	12.19029	0.83248	0.49367	0.01346	2619.2	32.04	2586.5	29.04	2643.6	30.44
27	EHV594-18	13.41925	1.13336	0.50709	0.01428	2709.6	39.9	2644.2	30.55	2689.6	32.88
28	EHV594-04	13.00141	0.78352	0.51324	0.01382	2679.8	28.41	2670.4	29.46	2673.2	27.87
29	EHV594-02	13.37218	1.15692	0.53662	0.01526	2706.3	40.87	2769.3	32.01	2617	32.22
30	EHV594-07	22.52342	1.26158	0.63293	0.01684	3206.6	27.23	3161.1	33.26	3206.6	25.43
31	EHV594-01	24.36363	1.39016	0.6736	0.018	3283.1	27.83	3319.8	34.66	3218	25.13
32	EHV594-34	7.00127	0.40856	0.36208	0.00966	2111.6	25.92	1992	22.87	2246.5	34.54
33	EHV594-22	4.94922	0.31242	0.295	0.00802	1810.7	26.66	1666.5	19.95	1923.3	35.89
34	EHV594-06	9.00522	0.47426	0.40266	0.01074	2338.5	24.07	2181.3	24.67	2531.3	27.88
35	EHV594-37	4.31803	0.31448	0.27653	0.0077	1696.8	30.02	1573.9	19.42	1843	42.29
36	EHV594-41	4.56951	0.30604	0.28155	0.0077	1743.7	27.9	1599.1	19.36	1942.4	40.58
37	EHV594-25	7.40995	0.47568	0.35232	0.00956	2162.2	28.72	1945.7	22.81	2376.3	33.46
38	EHV594-10	7.52917	0.42356	0.32475	0.00876	2176.5	25.21	1812.9	21.29	2602.3	29.1
39	EHV594-17	7.41461	0.43828	0.30995	0.00836	2162.7	26.44	1740.5	20.59	2534.1	30.68
40	EHV594-42	4.75362	0.29362	0.25044	0.00676	1776.7	25.91	1440.8	17.42	2146.1	38.32
41	EHV594-15	5.54236	0.27934	0.27309	0.00724	1907.2	21.68	1556.5	18.34	2321	29.75
42	EHV594-21	9.10419	0.70816	0.32679	0.00928	2348.5	35.58	1822.8	22.54	2851.8	33.69
43	EHV594-05	11.13585	0.53226	0.35199	0.00932	2534.6	22.27	1944.1	22.22	3085.7	25.47

Table 7. *(Continued.)*

	Disc (%)	Pb (ppm)	Th (ppm)	U (ppm)	Th/U	Accepted age (Ma)	1σ
1	−9.5	37.53	132.49	484	0.3	522.2	25.13
2	2.5	294.57	438.41	1156.72	0.4	1576.5	18.7
3	1.0	404.96	2834.73	1472.53	1.9	1687.3	19.69
4	7.3	31.81	53.2	115.21	0.5	1693.1	22.03
5	10.8	144.87	217.51	516.88	0.4	1715.6	20.34
6	0.2	355.16	219.86	1262.73	0.2	1720.9	20.07
7	4.7	68.88	241.29	244.75	1.0	1721.7	21.18
8	7.7	114.84	201.38	398.96	0.5	1756.4	20.56
9	8.0	50.99	82.57	175.92	0.5	1766.8	21.68
10	6.3	67.79	169.02	233.57	0.7	1769.2	21.29
11	5.6	61.67	110.36	206.35	0.5	1815	21.93
12	3.4	124.52	117.91	411.87	0.3	1833	21.69
13	−1.8	111.54	127.45	365.73	0.3	1847.1	21.83
14	−2.8	49.75	71.27	163.08	0.4	1847.5	22.98
15	3.0	226.01	718.14	738.6	1.0	1852.4	21.54
16	0.7	82.95	144.37	270.04	0.5	1858.7	22.04
17	−1.3	54.61	98.07	175.14	0.6	1883	22.9
18	−1.7	201.79	191.16	643.39	0.3	1892.5	21.92
19	−3.0	84.47	92.74	267.28	0.3	1904.9	22.99
20	−0.5	81.62	98.37	257.77	0.4	1908.3	22.55
21	−3.1	102.83	156.99	324.14	0.5	1911.5	22.31
22	−3.7	46.73	51.04	146.39	0.3	1921.5	32.01
23	6.9	65.72	205.95	159.52	1.3	2387.3	28.09
24	1.4	87.74	159.22	205.91	0.8	2455.6	27.88
25	1.0	74.34	85.31	165.76	0.5	2561.5	30.07
26	2.2	89.97	106.08	198.3	0.5	2586.5	29.04
27	1.7	51.81	158.41	111.16	1.4	2644.2	30.55
28	0.1	103.73	281.81	219.93	1.3	2673.2	27.87
29	−5.8	44.02	61.7	89.27	0.7	2769.3	25.43
30	1.4	158.11	137.87	271.81	0.5	3206.6	25.43
31	−3.2	151.38	96.26	244.54	0.4	3218	25.13
32	**11.3**	**184.95**	**305.63**	**555.73**	**0.5**	**NA**	**NA**
33	**13.4**	**89.59**	**160.84**	**330.41**	**0.5**	**NA**	**NA**
34	**13.8**	**136.77**	**483.01**	**369.59**	**1.3**	**NA**	**NA**
35	**14.6**	**62.5**	**151.36**	**245.87**	**0.6**	**NA**	**NA**
36	**17.7**	**97.44**	**348.92**	**376.5**	**0.9**	**NA**	**NA**
37	**18.1**	**184.31**	**453.93**	**569.18**	**0.8**	**NA**	**NA**
38	**30.3**	**177.73**	**1300.79**	**595.47**	**2.2**	**NA**	**NA**
39	**31.3**	**93.46**	**286.22**	**328.07**	**0.9**	**NA**	**NA**
40	**32.9**	**260.38**	**813.44**	**1131.06**	**0.7**	**NA**	**NA**
41	**32.9**	**224.41**	**216.22**	**894.09**	**0.2**	**NA**	**NA**
42	**36.1**	**59.36**	**225.81**	**197.62**	**1.1**	**NA**	**NA**S
43	**37.0**	**186.67**	**71.88**	**577.07**	**0.1**	**NA**	**NA**

NA – Not Applicable – Bold data are rejected and not utilised in the analysis. Discordance is defined as $1 - (^{206}\text{Pb}/^{238}\text{U}$ Age $\div\ ^{207}\text{Pb}/^{206}\text{Pb}$ Age).

(Dobmeier *et al.* 2006) and from pegmatites in the Nellore schist belt (Ghosh *et al.* 1994). Combining the results from the two samples (EHV591 and EHV594), we interpret that the Khammam belt of NKSB represents Archaean protolith (>2600 Ma), which has been affected by four major tectonothermal events which has affected/reset the U–Pb geo-chronometer in zircons. The first event at 2500–2600 Ma could be associated with the first amalgamation of the NKSB with the Dharwar craton, as indicated by the granite event in the KGB and the widespread granitic event in the Dharwar craton (Jayananda *et al.* 2013). This event is also represented by granite magmatism and zircon rim ages in the KGB (Santosh *et al.* 2004). We propose that the terranes were juxtaposed at 2600–2500 Ma to form an integral part of proto-India. The 1800–1900 Ma event identified

Table 8. *Results of U–Pb analysis of the zircons from sample EHV591 from the Khammam belt of NKSB.*

Grain-ID	Isotopic ratios				Ages (Ma)						Disc (%)	Pb (ppm)	Th (ppm)	U (ppm)	Th/U	Accepted age (Ma)	1σ
	$^{207}Pb/^{235}U$	2σ	$^{206}Pb/^{238}U$	2σ	$^{207}Pb/^{235}U$	1σ	$^{206}Pb/^{238}U$	1σ	$^{207}Pb/^{206}Pb$	1σ							
EHV591-12	0.62422	0.09802	0.07704	0.00306	492.5	30.64	478.5	9.18	533.5	138.76	10.3	199.88	150.33	82.59	1.8	478.5	9.18
EHV591-50	7.58892	1.04078	0.36494	0.01214	2183.6	61.52	2005.5	28.65	2221.5	57.71	9.7	95.17	149.55	283.6	0.5	2005.5	28.65
EHV591-48	8.01961	0.68808	0.39224	0.01126	2233.2	38.73	2133.2	26.06	2392.7	43.95	10.8	73.61	265.05	204.08	1.3	2133.2	26.06
EHV591-21	7.78657	0.62534	0.39818	0.0112	2206.7	36.13	2160.7	25.81	2333.9	37.47	7.4	23.01	142.52	148	1.0	2160.7	25.81
EHV591-49	8.79523	0.6763	0.41105	0.01146	2317	35.05	2219.7	26.2	2349.3	42.38	5.5	189.13	469.15	500.37	0.9	2219.7	26.2
EHV591-09	8.96995	0.93798	0.42036	0.01256	2335	47.76	2262.1	28.5	2383.8	40.72	5.1	186.06	151.36	72.3	2.1	2262.1	28.5
EHV591-11	8.64413	1.07564	0.42201	0.0135	2301.2	56.62	2269.6	30.62	2418.6	46.33	6.2	5.85	127.1	50.46	2.5	2269.6	30.62
EHV591-55	8.79161	0.82928	0.42363	0.01242	2316.6	43	2276.9	28.12	2384.2	47.32	4.5	57.55	231.3	147.74	1.6	2276.9	28.12
EHV591-51	8.81442	0.85414	0.424	0.0125	2319	44.18	2278.6	28.31	2391.3	46.72	4.7	68.94	117.33	176.82	0.7	2278.6	28.31
EHV591-39	9.65928	1.56126	0.4248	0.01524	2402.8	74.36	2282.2	34.46	2525	57.04	9.6	9.61	66.06	32.12	2.1	2282.2	34.46
EHV591-27	8.04031	1.72554	0.42648	0.01834	2235.6	96.9	2289.8	41.45	2351.3	76.53	2.6	50.92	33.3	18.74	1.8	2289.8	41.45
EHV591-29	9.49723	0.87412	0.42802	0.01234	2387.3	42.28	2296.8	27.87	2452	39.7	6.3	98.13	128.23	161.18	0.8	2296.8	27.87
EHV591-33	9.27771	0.6173	0.43244	0.01172	2365.8	30.49	2316.7	26.37	2439.7	35.93	5.0	247.79	329.44	332.9	1.0	2316.7	26.37
EHV591-57	9.79114	1.68464	0.43493	0.016	2415.3	79.26	2327.9	35.92	2447.3	63.4	4.9	10.48	44.68	26.21	1.7	2327.9	35.92
EHV591-13	8.93366	0.48868	0.43289	0.01142	2331.2	24.98	2318.8	25.67	2377.8	30.38	2.5	20.59	110.72	502.01	0.2	2331.2	24.98
EHV591-47	10.12817	0.93366	0.43962	0.0127	2446.5	42.6	2348.9	28.42	2439	43.69	3.7	77.26	92.64	191.13	0.5	2348.9	28.42
EHV591-03	9.75075	0.61396	0.44421	0.01192	2411.5	28.99	2369.5	26.59	2467.2	30.55	4.0	109.75	375.78	268.58	1.4	2369.5	26.59
EHV591-18	9.53649	0.58798	0.4445	0.01188	2391.1	28.33	2370.8	26.52	2447.4	31.89	3.1	32.38	367.92	385.2	1.0	2370.8	26.52
EHV591-04	9.59945	1.69188	0.44681	0.01672	2397.1	81.04	2381.1	37.23	2466.7	57.95	3.5	128.57	54.64	23.38	2.3	2381.1	37.23
EHV591-28	10.63725	1.13348	0.448	0.0134	2492	49.45	2386.4	29.82	2535.9	41.45	5.9	63.44	112.17	123.59	0.9	2386.4	29.82
EHV591-32	10.60833	1.23674	0.44809	0.01366	2489.4	54.09	2386.8	30.4	2400.1	44.89	0.6	132.38	88.51	61.71	1.4	2386.8	30.4
EHV591-56	9.3031	0.8069	0.44885	0.0129	2368.3	39.76	2390.2	28.68	2430.7	45.79	1.7	81.14	196.84	196.59	1.0	2390.2	28.68
EHV591-01	10.17076	1.26414	0.44927	0.0141	2450.4	57.45	2392	31.37	2439.9	43.72	2.0	21.87	129.18	52.91	2.4	2392	31.37
EHV591-23	9.62693	0.54194	0.4408	0.01166	2399.7	25.89	2354.2	26.07	2401.4	32.08	2.0	15.69	108.51	1033.89	0.1	2399.7	25.89
EHV591-40	9.48815	0.95452	0.45221	0.0134	2386.4	46.21	2405.1	29.72	2426.4	43.88	0.9	43.19	92.76	103.86	0.9	2405.1	29.72
EHV591-35	9.88137	0.5926	0.45282	0.0121	2423.8	27.65	2407.8	26.84	2455.9	35.18	2.0	199.02	297.09	595.07	0.5	2407.8	26.84
EHV591-31	9.53787	0.67546	0.45439	0.01242	2391.2	32.54	2414.7	27.5	2385	36.36	−1.2	25.43	135.73	234.84	0.6	2414.7	27.5
EHV591-05	9.71745	0.60214	0.45556	0.0122	2408.4	28.52	2419.9	27	2454.8	30.5	1.4	335.09	308.4	306.8	1.0	2419.9	27

Table 8. *(Continued.)*

	Isotopic ratios				Ages (Ma)						Disc	Pb	Th	U	Th/U	Accepted	
Grain-ID	$^{207}Pb/^{235}U$	2σ	$^{206}Pb/^{238}U$	2σ	$^{207}Pb/^{235}U$	1σ	$^{206}Pb/^{238}U$	1σ	$^{207}Pb/^{206}Pb$	1σ	(%)	(ppm)	(ppm)	(ppm)		age (Ma)	1σ
EHV591-43	9.61677	0.93348	0.45583	0.01336	2398.8	44.64	2421.1	29.6	2425.2	43.98	0.2	40.53	118.79	96.7	1.2	2421.1	29.6
EHV591-24	10.58825	1.65512	0.45848	0.0159	2487.7	72.51	2432.8	35.14	2512.1	52.31	3.2	440.65	99.54	37.21	2.7	2432.8	35.14
EHV591-02	9.80943	0.72434	0.45871	0.0126	2417	34.02	2433.9	27.86	2449.1	32.64	0.6	65.06	135.35	154.19	0.9	2433.9	27.86
EHV591-54	9.62265	1.088	0.46023	0.01422	2399.3	52	2440.6	31.39	2465.6	49.82	1.0	36.77	67.36	86.89	0.8	2440.6	31.39
EHV591-36	10.10271	0.6425	0.4613	0.0124	2444.2	29.38	2445.3	27.37	2408.6	36.09	−1.5	16.01	621.99	469.17	1.3	2445.3	27.37
EHV591-10	10.19262	0.56488	0.46487	0.01226	2452.4	25.62	2461	26.98	2477.5	29.57	0.7	19.59	257.05	435.13	0.6	2452.4	25.62
EHV591-20	10.25313	0.61466	0.46357	0.01232	2457.9	27.73	2455.3	27.15	2423.7	31.81	−1.3	54.2	219.98	507.02	0.4	2455.3	27.15
EHV591-06	10.25166	0.52432	0.4556	0.01192	2457.8	23.66	2420.1	26.4	2443.5	28.67	1.0	67.42	570.45	799.56	0.7	2457.8	23.66
EHV591-22	9.52064	1.2039	0.46425	0.0148	2389.5	58.1	2458.3	32.56	2414	46.76	−1.8	419.13	93.97	53.9	1.7	2458.3	32.56
EHV591-59	10.00302	0.73052	0.46455	0.0129	2435.1	33.71	2459.6	28.38	2426.1	44.4	−1.4	252.58	527.3	591.3	0.9	2459.6	28.38
EHV591-45	10.62095	0.7809	0.46667	0.01286	2490.5	34.12	2468.9	28.28	2476.2	39.81	0.3	280.51	420.44	653.69	0.6	2468.9	28.28
EHV591-25	10.41998	0.58076	0.48464	0.0128	2472.8	25.82	2547.4	27.79	2464.3	32.07	−3.4	45.11	330.06	988.69	0.3	2472.8	25.82
EHV591-52	9.81684	1.2243	0.46804	0.01494	2417.7	57.46	2474.9	32.82	2472.2	51.64	−0.1	25.81	78.13	59.97	1.3	2474.9	32.82
EHV591-53	13.70931	3.232	0.46909	0.01904	2729.8	111.55	2479.6	41.79	2424.4	71.11	−2.3	11.95	64.66	27.71	2.3	2479.6	41.79
EHV591-16	10.67599	0.55032	0.45291	0.01186	2495.3	23.93	2408.2	26.32	2565.4	29.48	6.1	61.38	350.04	724.32	0.5	2495.3	23.93
EHV591-42	9.69543	1.16472	0.47346	0.01482	2406.3	55.29	2498.7	32.43	2412.9	48.53	−3.6	25.09	58.26	57.64	1.0	2498.7	32.43
EHV591-19	10.03918	1.13646	0.47475	0.01446	2438.4	52.27	2504.3	31.58	2417.3	42.44	−3.6	216.17	114.24	74.15	1.5	2504.3	31.58
EHV591-46	10.28973	0.75868	0.48323	0.01336	2461.2	34.12	2541.3	29.02	2468.5	40.2	−2.9	233.59	798.42	525.7	1.5	2541.3	29.02
EHV591-38	21.10298	2.45302	0.57812	0.01742	3143.3	56.34	2941.1	35.58	3163.6	38.82	7.0	12.55	31.37	77.21	0.4	2941.1	35.58
EHV591-26	20.47662	2.26494	0.61005	0.01806	3114.1	53.54	3070.2	36.17	3096.1	35.83	0.8	7.35	30.42	80.4	0.4	3070.2	36.17
EHV591-60	20.31353	1.74678	0.62156	0.01772	3106.4	41.61	3116.1	35.21	3171.6	42.37	1.7	129.2	110.2	226.05	0.5	3116.1	35.21
EHV591-07	**6.60959**	**0.45918**	**0.35566**	**0.00974**	**2060.6**	**30.63**	**1961.5**	**23.18**	**2212.2**	**34.5**	**11.3**	**1311.1**	**147.76**	**206.08**	**0.7**	NA	NA
EHV591-08	**9.52912**	**0.50772**	**0.32338**	**0.00848**	**2390.4**	**24.48**	**1806.2**	**20.67**	**2414.8**	**29.34**	**25.2**	**27.95**	**660.38**	**4407.68**	**0.1**	NA	NA
EHV591-14	**7.84222**	**0.85932**	**0.3756**	**0.01158**	**2213.1**	**49.34**	**2055.7**	**27.15**	**2433.3**	**43.6**	**15.5**	**134.08**	**56.73**	**59.6**	**1.0**	NA	NA
EHV591-15	**4.82996**	**0.2562**	**0.22126**	**0.00588**	**1790.1**	**22.31**	**1288.5**	**15.5**	**2435.9**	**31.28**	**47.1**	**301.72**	**147.82**	**658.84**	**0.2**	NA	NA
EHV591-17	**0.63542**	**0.04308**	**0.05502**	**0.00158**	**499.5**	**13.38**	**345.3**	**4.85**	**1324.5**	**53.63**	**73.9**	**157.47**	**440.51**	**1212.9**	**0.4**	NA	NA
EHV591-37	**3.80904**	**0.44718**	**0.25027**	**0.0081**	**1594.7**	**47.21**	**1439.9**	**20.9**	**1784.2**	**61.31**	**19.3**	**41.05**	**41.43**	**69.55**	**0.6**	NA	NA
EHV591-41	**3.76707**	**0.53884**	**0.23115**	**0.00826**	**1585.8**	**57.39**	**1340.5**	**21.61**	**1833.5**	**72.24**	**26.9**	**10.75**	**35.19**	**50.57**	**0.7**	NA	NA
EHV591-44	**7.35577**	**0.68586**	**0.37353**	**0.01094**	**2155.6**	**41.67**	**2046**	**25.69**	**2301.7**	**45.5**	**11.1**	**53.1**	**113.83**	**154.6**	**0.7**	NA	NA

NA: Not Applicable. Bold data are rejected and not utilised in the analysis. Discordance is defined as $1 - (^{206}Pb/^{238}U\ \text{Age} \div\ ^{207}Pb/^{206}Pb\ \text{Age})$.
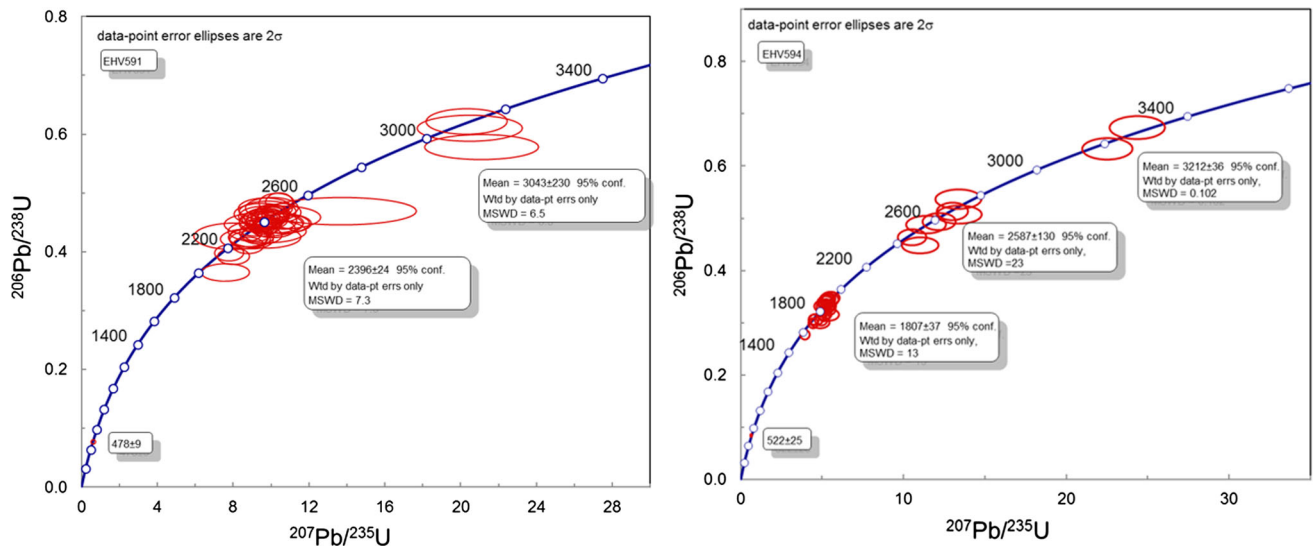
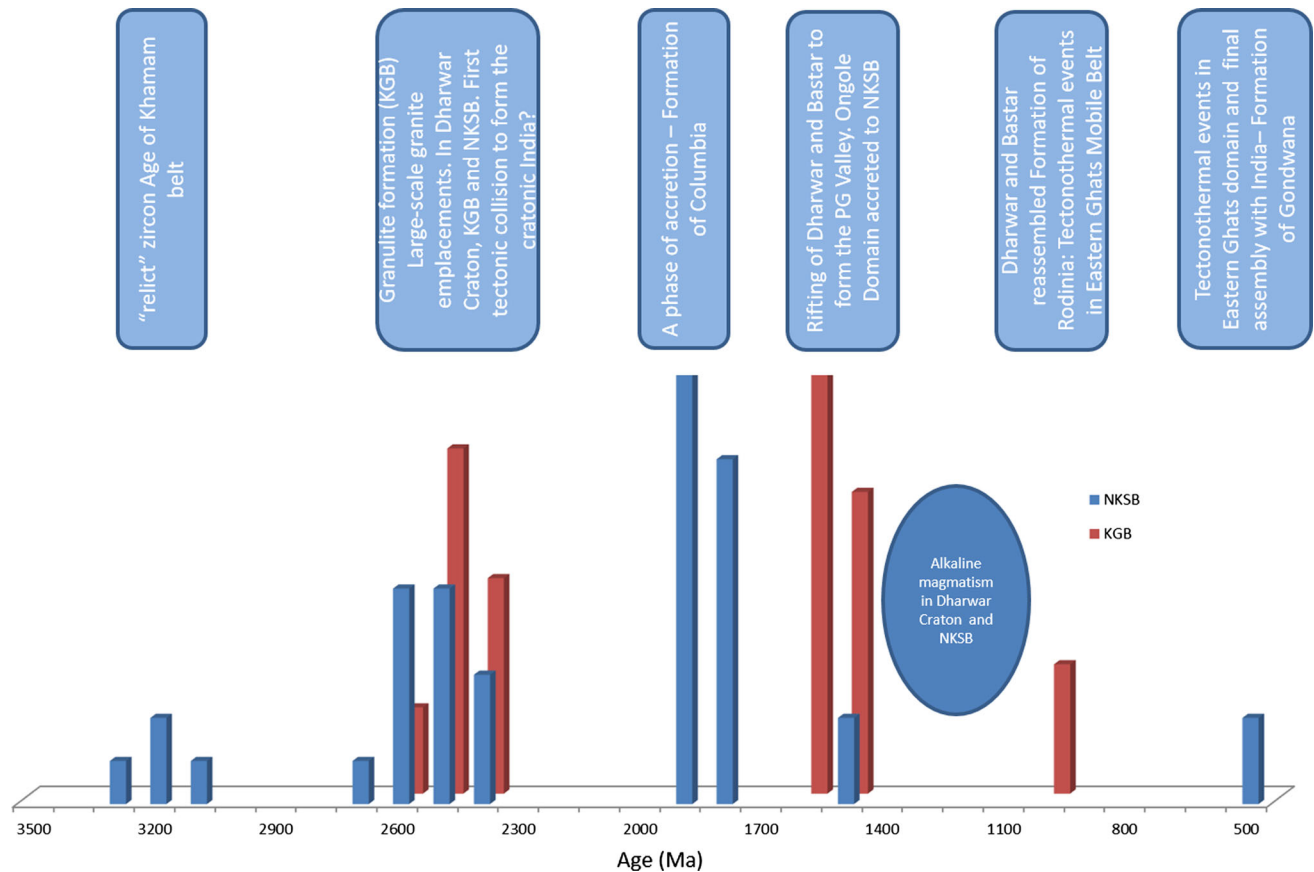Figure 6. U–Pb concordia diagram of zircons from the Khammam schist belt of NKSB.

Figure 7. Summary of age groups obtained in the study with regional events. The height of the individual bars is proportional to the number of grains within that age group.

in this study, combined with previously reported events from the Nellore schist belt (Vadlamani 2010; Vadlamani *et al.* 2012; Das *et al.* 2015), support another continental accretion event in the eastern part of the southern Indian craton as proposed by Saha *et al.* (2015). The ∼1600 Ma event is considered to represent suturing of the Ongole domain with the Nellore schist belt (Bose *et al.* 2011; Vijaya Kumar *et al.* 2011; Henderson *et al.* 2013) and this event is evident in sample

EHV594 (figure 6). The ∼1000 Ma event from the NKSB (Yoshida *et al.* 1996; Okudaira *et al.* 2001) was not identified in the present study. However, zircons from the NKSB show evidence of the ∼500 Ma Pan-African event that led to the formation of Gondwana (figures 6 and 7).

7. Conclusions

The northern part of the Nellore–Khammam schist belt known as the Khammam schist belt, and the Karimnagar granulite belt, which are juxtaposed at a high angle to each other are unique in terms of their tectonothermal evolution, as recorded by U–Pb zircon age patterns.

Southern India has been affected by multiple events of rifting and collision-accretion throughout its Proterozoic history (see also Basu and Bickford 2015; Saha *et al.* 2015). The present study indicates that the Khammam schist belt and the northern part of the NKSB probably formed part of cratonic India by about 2500 Ma. The Dharwar and Bastar cratons amalgamation was initiated at ∼2600 Ma with the formation of the granulites and culminating with the emplacement of the granites at ∼2400 Ma. The schist belt has experienced another orogenic accretion at about 1900 Ma probably assigned to the formation of Columbia. The Dharwar and Bastar cratons separated to form the P–G valley at ∼1600 Ma along with the metamorphic resetting of zircons within the KGB and BGB granulites and gneisses. During this same time period (∼1600 Ma), at an orthogonal direction to P–G valley, accretion tectonics would have been ongoing whereby the Ongole domain was accreted to the NKSB (Henderson *et al.* 2013). The P–G valley area inverted to be under a compressional regime, resulting in closure of the basin and the reassembly of the Dharwar and Bastar cratons at about 1000 Ma, which could be linked to the formation of Rodinia. The NKSB was affected by the late Pan-African tectonothermal event at ca. 500 Ma that possibly marked the final episode of its assembly with the Eastern Ghats province of the EGMB, since then forming part of the present day Indian subcontinent.

Our study highlights that plate accretion and rifting events in the eastern part of the Dharwar craton and between the Dharwar and Bastar cratons have been repeated through time with highly complex events. Southern India's present tectonic configuration is the result of multiple tectonic events between 2500 and 500 Ma, which occurred in different areas and at different times, which can potentially be linked to the formation and dispersal of three supercontinents.

Acknowledgements

References

Acharyya S K 2003 A plate tectonic model for Proterozoic crustal evolution of central Indian tectonic zone; *Geol. Mag.* **7** 9–31.

Balasubrhamanyan M N 2006 Geology and tectonics of India: An overview; *Int. Assoc. Gondwana Res. Mem.* **9**.

Basu A and Bickford M E 2015 An alternate perspective of the opening and closing of the intracratonic Purana basins in peninsular India; *J. Geol. Soc. India* **85** 5–25.

Belica M E, Piispa E J, Meert J G, Pesonenc L J, Plado J, Pandit M, Kamenova G D and Celestinoa M 2014 Paleoproterozoic mafic dyke swarms from the Dharwar craton; paleomagnetic poles for India from 2.37–1.88 Ga and rethinking the Columbia supercontinent. *Precamb. Res.* **244** 100–122.

Biswal T K, De Waele B and Ahuja H 2007 Timing and dynamics of the juxtaposition of the Eastern Ghats Mobile Belt against the Bhandara Craton, India: A structural and zircon U-Pb SHRIMP study of the fold-thrust belt and associated nepheline syenite plutons; *Tectonics* **26** 1–21.

Bleeker W 2003 The late Archaean record: A puzzle in *c.* 35 pieces; *Lithos* **71** 99–134.

Bose S, Dunkley D J, Dasgupta S, Das K and Arima M 2011 India–Antarctica–Australia–Laurentia connection in the Paleoproterozoic–Mesoproterozoic revisited: Evidence from new zircon U–Pb and monazite chemical age data from the Eastern Ghats Belt, India; *Geol. Soc. Am. Bull.* **123** 2031–2049.

Bradley D C 2011 Secular trends in the geologic record and the supercontinent cycle; *Earth-Sci. Rev.* **108** 16–33.

Carson C J, Ague J J and Coath C D 2002 U–Pb geochronology from Tonagh Island, East Antarctica: Implication for the timing of ultra-high temperature metamorphism of the Napier complex; *Precamb. Res.* **116** 237–263.

Chadwick B, Vasudev V N and Hegde G V 2000 The Dharwar craton, southern India, interpreted as the result of late Archean oblique convergence; *Precamb. Res.* **99** 91–111.

Chalapathi Rao N V and Srivastava R K 2016 Kimberlites, lamproites, lamprophyres, carbonatites, other alkaline rocks and mafic dykes from the Indian Shield: Glimpses of research (2012–2016); *Proc. Indian Nat. Sci. Acad.* **82** 515–536.

Chalapathi Rao N V, Wu F Y, Mitchell R H, Li Q L and Lehmann B 2013 Mesoproterozoic U-Pb ages, trace element and Sr-Nd isotopic composition of perovskite from kimberlites of the Eastern Dharwar craton, southern India: Distinct mantle sources and a widespread 1.1 Ga tectonomagmatic event; *Chem. Geol.* **353** 48–64.

Chaudhuri A K and Chanda S K 1991 The Proterozoic basin of Pranhita-Godavari valley: An overview; In: *Sedimentary basins of India: Tectonic context* (eds) Tandon S K, Pant C C and Casshyap S B, Ganodaya Prakashan, Nainital, pp. 13–30.

Chaudhuri A K, Deb G K, Patranabis-Deb S and Sarkar S 2012 Paleogeographic and tectonic evolution of the Pranhita-Godavari valley, central India: A stratigraphic perspective; *Am. J. Sci.* **312** 766–815.

Chaudhuri A K, Saha D, Deb G K, Patranabis-Deb S, Mukherjee M K and Ghosh G 2002 The Purana Basins of Southern Cratonic Province of India: A case for mesoproterozoic fossil rifts; *Gondwana Res.* **5** 23–33.

Conrad J E, Hein J R, Chaudhuri A K, Patranabis-Deb S, Mukhopadhyay J, Deb G K and Beukes N J 2011 Constraints on the development of Proterozoic basins in central India from $^{40}Ar/^{39}Ar$ analysis of authigenic glauconitic minerals; *Geol. Soc. Am. Bull.* **123(1/2)** 158–167.

Crawford A R 1969 India, Ceylon and Pakistan: New age data and comparisons with Australia; *Nature* **233** 380–384.

Das K, Yokoyama K, Chakraborty P P and Sarkar A 2009 Basal tuffs and contemporaneity of the Chattisgarh and Khariar basins based on new dates and geochemistry; *J. Geol.* **117** 88–102.

Das S, Shukla D, Bhattacharjee S and Mitra S K 2015 Age constraints of Udayagiri domain of Nellore schist belt by xenotime dating around Pamuru, Prakasam district, Andhra Pradesh; *J. Geol. Soc. India* **85** 289–298.

Dasgupta S, Bose S, Bhowmik S K and Sengupta P 2017 The Eastern Ghats Belt, India, in the context of supercontinent assembly; In: Crustal evolution of India and Antarctica: The supercontinent connection (eds) Pant N C and Dasgupta S, *Geol. Soc. London, Spec. Publ.* **457** 87–104.

Demirer K 2012 U–Pb Baddeleyite ages from mafic dyke swarms in Dharwar Craton, India: Links to an ancient supercontinent; Dissertations in Geology at Lund University, Master's thesis, 308p.

Dharma Rao C V, Santosh M and Wu Y 2011a Mesoproterozoic ophiolitic mélange from the SE periphery of the Indian plate: U–Pb zircon ages and tectonic implications; *Gondwana Res.* **19** 384–401.

Dharma Rao C V, Windley B F and Choudhary A K 2011b The Chimalpahad anorthosite complex and associated basaltic amphibolites, Nellore Schist Belt, India: Magma chamber and roof of a Proterozoic island arc; *J. Asian Earth Sci.* **40** 1027–1043.

Dobmeier C and Raith M 2003 Crustal architecture and evolution of the Eastern Ghats Belt and adjacent regions of India; In: Proterozoic east Gondwana: Supercontinent assembly and breakup (eds) Yoshida M, Windley B F and Dasgupta S, *Geol. Soc. London, Spec. Publ.* **206** 145–168.

Dobmeier C, Lutke S, Hammerschmidt K and Mezger K 2006 Emplacement and deformation of the Vinukonda

meta-granite (Eastern Ghats, India) – Implications for the geological evolution of peninsular India and for Rodinia reconstructions; *Precamb. Res.* **146** 165–178.

French J E and Heaman L M 2010 Precise U-Pb dating of Paleoproterozoic mafic dyke swarms of the Dharwar craton, India: Implications for the existence of the Neoarchean supercraton Sclavia; *Precamb. Res.* **183** 416–441.

French J E, Heaman L M, Chacko T and Rivard B 2004 Global mafic magmatism and continental breakup at 2.2 Ga: Evidence from the Dharwar craton, India; *Abstracts Geol. Soc. Am.* **36** 340p.

Friend C R L and Nutman A P 1991 SHRIMP U–Pb geochronology of the Closepet Granite and peninsular gneiss, Karnataka, south India; *J. Geol. Soc. India* **38** 357–368.

Ghosh D, Das J N, Rao A K, Ray Barman T, Kollapuri V K and Sarkar A 1994 Fission-track and K–Ar dating of pegmatite and associated rocks of Nellore schist belt, Andhra Pradesh: Evidence of Middle to Late Proterozoic events; *Indian Mineral.* **48** 95–102.

Halls H C, Kumar A, Srinivasan R and Hamilton M A 2007 Paleomagnetism and U/Pb geochronology of easterly trending dykes in the Dharwar Craton, India: Feldspar clouding, radiating dyke swarms and the position of India at 2.37 Ga; *Precamb. Res.* **155** 47–68.

Hari Prasad B, Okudaira T, Hayasaka Y, Yoshida M and Divi R S 2000 Petrology and geochemistry of amphibolites from the Nellore–Khammam schist belt, SE India; *J. Geol. Soc. India* **56** 67–78.

Henderson B, Collins A, Payne J, Forbes C and Saha D 2013 Geologically constraining India in Columbia: The age, isotopic provenance and geochemistry of the protoliths of the Ongole Domain, Southern Eastern Ghats, India; *Gondwana Res.* **26** 888–906.

Holland T H 1907 *The imperial gazetteer of India*; 1st edn, Oxford At The Clarendon Press, pp. 50–103.

Jackson S E, Pearson N J, Griffin W L and Belousova E A 2004 The application of laser ablation-inductively coupled plasma-mass spectrometry to *in situ* U–Pb zircon geochronology; *Chem. Geol.* **211** 47–69.

Jayananda M, Kano T, Peucat J J and Channabasappa S 2008 3.35 Ga komatiite volcanism in the western Dharwar craton, southern India: Constraints from Nd isotopes and whole rock geochemistry; *Precamb. Res.* **162** 160–179.

Jayananda M, Peucat J J, Chardon D, Krishna Rao B, Fanning C M and Corfu F 2013 Neoarchean greenstone volcanism and continental growth, Dharwar craton, southern India: Constraints from SIMS U–Pb zircon geochronology and Nd isotopes; *Precamb. Res.* **227** 55–76.

Joy S, Jelsma H, Armstrong R and Tappe S 2015 SHRIMP U–Pb zircon provenance of the Sullavai Group of Pranhita–Godavari basin and Bairenkonda formation of Cuddapah basin, with implications for the southern Indian Proterozoic tectonic architecture; *J. Asian Earth Sci.* **111** 827–839.

Kale V S and Phansalkar V G 1991 Purana basins of peninsular India: A review; *Basin Res.* **3** 1–36.

Korhonen F J, Saw A K, Clark C, Brown M and Bhattacharya S 2011 New constraints on UHT metamorphism in the Eastern Ghats Province through the application

of phase equilibria modelling and in situ geochronology; *Gondwana Res.* **20** 764–781.

Kovach V P, Simmat R, Rickers K, Berezhnaya N G, Salnikova E B, Dobmeier C, Raith M M, Yakovleva S Z and Kotov A B 2001 The Western Charnockite Zone of the Eastern Ghats Belt, India – an independent crustal province of Late Archaean (2.8 Ga) and Palaeoproterozoic (1.7–1.6 Ga) terrains; *Gondwana Res.* **4** 666–667.

Kumar A, Heaman L M and Manikyamba C 2007 Mesoproterozoic kimberlites in South India: A possible link to 1.1 Ga global magmatism; *Precamb. Res.* **154** 192–204.

Kumar A, Hamilton M A and Halls H C 2012a A Paleoproterozoic giant radiating dyke swarm in the Dharwar Craton, southern India; *Geochem. Geophys. Geosyst.* **13(2)**, https://doi.org/10.1029/2011GC003926.

Kumar A, Nagaraju E, Besse J and Bhaskar Rao Y J 2012b New age, geochemical and paleomagnetic data on a 2.21 Ga dyke swarm from south India: Constraints on Paleoproterozoic reconstruction; *Precamb. Res.* **220–221** 123–138.

Kumar A, Parashuramulu V and Nagaraju E 2015 A 2082 Ma radiating dyke swarm in the Eastern Dharwar Craton, southern India and its implications to Cuddapah basin formation; *Precamb. Res.* **266** 490–505.

Ludwig K R 2001 Isoplot 3.0, a geochronological toolkit for Microsoft Excel; Special Publication No. 4, Berkeley Geochronology Center, Berkeley, California, pp. 1–70.

Ma M, Wan Y, Santosh M, Xu Z, Xie H, Dong C, Liu D and Guo C 2012 Decoding multiple tectonothermal events in zircon from single rock samples: SHRIMP zircon U–Pb data from the late Neoarchean rocks of Daquingshan, North China Craton; *Gondwana Res.* **22** 810–827.

Mallikarjuna R J, Bhattacharji S, Rao M N and Hermes O D 1995 ^{40}Ar–^{39}Ar ages and geochemical characteristics of dolerite dykes around the Proterozoic Cuddapah basin, South India; In: Mafic dyke swarms of Peninsular India (ed.) Devaraju T C, *Geol. Soc. India. Memoir* **33** 307–328.

Malone S J, Meert J G, Banerjee D M, Pandit M K, Tamrat E, Kamenov G D, Pradhan V R and Sohl L E 2008 Paleomagnetism and detrital zircon geochronology of the upper Vindhyan Sequence, Son Valley and Rajasthan, India: A ca. 1000 Ma closure age for the Purana basins; *Precamb. Res.* **164** 137–159.

Meert J G 2012 What's in a name? The Columbia (Paleopangaea/Nuna) supercontinent; *Gondwana Res.* **21** 987–993.

Meert J G, Pandit M K, Pivarunas A, Katusin K and Sinha A K 2017 India and Antarctica in the Precambrian: A brief analysis; In: *Crustal evolution of India and Antarctica: The supercontinent connection* (eds) Pant N C and Dasgupta S, *Geol. Soc. London, Spec. Publ.* **457**, https://doi.org/10.1144/SP457.13.

Moeen S 1998 P–T estimates from the Nellore schist belt (India) and evidence for superimposed metamorphic events; *Geol. J.* **33** 1–15.

Mukhopadhyay D and Basak K 2009 The Eastern Ghats Belt–Polycyclic granulite terrane; *J. Geol. Soc. India* **73** 489–518.

Murthy Y G K, Baburao V, Guptasarma D, Rao J M and Rao M N 1987 Tectonic, petrochemical and geophysical studies of mafic dyke swarms around the Proterozoic Cud-

dapah basin, south India; In: *Mafic dyke swarms* (eds) Halls H C and Fahrig W F, *Geol. Assoc. Canada, Spec. Publ.* **34** 303–316.

Nance R D and Murphy J B 2013 Origin of the supercontinent cycle; *Geosci. Front.* **4** 439–448.

Nance D R, Murphy J B and Santosh M 2013 The supercontinent cycle: A retrospective essay; *Gondwana Res.* **25(1)** 4–29.

Naqvi S M and Rogers J J W 1987 *Precambrian Geology of India*; Oxford University Press, Oxford.

Naqvi S M, Divakara Rao V and Narain H 1974 The protocontinental growth of the Indian shield and the antiquity of its rift valleys; *Precamb. Res.* **1(4)** 345–389.

Okudaira T, Hamamoto T, Hari Prasad B and Kumar R 2001 Sm–Nd and Rb–Sr dating of amphibolite from the Nellore–Khammam schist belt, SE India: Constraints on the collision of the Eastern Ghats terrane and Dharwar–Bastar craton; *Geol. Mag.* **138** 495–498.

Pandey B K, Gupta J N, Sarma K J and Sastry C A 1997 Sm–Nd, Pb–Pb and Rb–Sr geochronology and petrogenesis of the mafic dyke swarm of Mahbubnagar, South India: Implications for Paleoproterozoic crustal evolution of the Eastern Dharwar Craton; *Precamb. Res.* **84** 181–196.

Patranabis-Deb S, Bickford M E, Hill B, Chaudhuri A K and Basu A 2007 SHRIMP ages of zircon in the uppermost tuff in Chattisgarh basin in central India require ∼500 Ma adjustment in Indian Proterozoic stratigraphy; *J. Geol.* **115** 407–415.

Pradhan V R, Pandit M K and Meert J G 2008 A cautionary note on the age of the paleomagnetic pole obtained from the Harohalli dyke swarms, Dharwar craton, southern India; In: *Indian dykes: Geochemistry, geophysics and geochronology* (eds) Srivastava R K, Shivaji C H and Chalapathi Rao N V, Narosa Publication, New Delhi, pp. 339–352.

Prakash D, Chandra Singh P, Tewari S, Joshi M, Frimmel H E, Hokada T and Rakotonandrasana T 2017 Petrology, pseudosection modelling and U–Pb geochronology of silica-deficient Mg–Al granulites from the Jagtiyal section of Karimnagar granulite terrane, northeastern Dharwar Craton, India; *Precamb. Res.* **299** 177–194.

Qureshy M N, Krishna Brahmam N, Garde S C and Mathur B K 1968 Gravity anomalies and the Godavari rift, India; *Geol. Soc. Am. Bull.* **79** 1221–1230.

Radhakrishna B P and Naqvi S M 1986 Precambrian continental crust of India and its evolution; *J. Geol.* **94** 145–166.

Rajesham T, Bhaskar Rao Y J and Murti K S 1993 The Karimnagar granulite terrane – a new sapphirine bearing granulite province, south India; *J. Geol. Soc. India* **4** 51–59.

Rakotonandrasana T 2017 Petrology, pseudosection modelling and U–Pb geochronology of silica-deficient Mg–Al granulites from the Jagtiyal section of Karimnagar granulite terrane, northeastern Dharwar Craton, India; *Precamb. Res.* **299** 177–194.

Ramakrishnan M 2003 Craton-mobile belt relations in Southern Granulite Terrain; *Geol. Soc. India Memoir* **50** 1–24.

Ramakrishnan M and Vaidyanadhan R 2008 *Geology of India*; Geological Society of India Bangalore, India.

Ramam P K and Murty V N 1997 *Geology of Andhra Pradesh*; Geological Society of India, Bangalore, India.

Rasmussen B, Bose P K, Sarkar S, Banerjee S, Fletcher I R and McNaughton N J 2002 1.6 Ga U-Pb zircon age for the Chorhat Sandstone, lower Vindhyan, India: Possible implications for early evolution of animals; *Geology* **30** 103–106.

Ratre K, De Waele B, Biswal T K and Sinha S 2010 SHRIMP geochronology for the 1450 Ma Lakhna dyke swarm: Its implications for the presence of Eoarchaean crust in the Bastar Craton and 1450–517 Ma depositional age for Purana basin (Kariar), Eastern Indian Peninsula; *J. Asian Earth Sci.* **39** 565–577.

Ray J S, Martin M W, Veizer J and Bowring S A 2002 U-Pb zircon dating and Sr isotope systematics of the Vindhyan Supergroup, India; *Geology* **30** 131–134.

Rickers K, Mezger K and Raith M M 2001 Evolution of the continental crust in the Proterozoic Eastern Ghats Belt, India and new constraints for Rodinia reconstruction: Implications from Sm–Nd, Rb–Sr and Pb–Pb isotopes; *Precamb. Res.* **112** 183–210.

Robinson P L 1971 A problem of faunal replacement on Permo-Triassic continents; *Palaeontology* **14** 131–153.

Rogers J J W 1986 The Dharwar craton and the assembly of peninsular India; *J. Geol.* **94** 129–143.

Rubatto D 2002 Zircon trace element geochemistry: Partitioning with garnet and the link between U-Pb ages and metamorphism; *Chem. Geol.* **184** 123–138.

Saha D 2011 Dismembered ophiolites in Paleoproterozoic nappe complexes of Kandra and Gurramkonda, south India; *J. Asian Earth Sci.* **42** 158–175.

Saha D and Mazumder R 2012 An overview of the Palaeoproterozoic geology of Peninsular India, and key stratigraphic and tectonic issues; In: *Palaeoproterozoic of India* (eds) Mazumder R and Saha D, *Geol. Soc. London, Spec. Publ.* **365** 5–29.

Saha D and Tripathy V 2012 Palaeoproterozoic sedimentation in the Cuddapah basin, south India and regional tectonics – a review; In: *Paleoproterozoic of India* (eds) Mazumder R and Saha D, *Geol. Soc. London, Spec. Publ.* **365** 159–182.

Saha D and Patranabis-Deb S 2014 Proterozoic evolution of Eastern Dharwar and Bastar cratons, India – an overview of the intracratonic basins, craton margins and mobile belts; *J. Asian Earth Sci.* **91** 230–251.

Saha D, Sain A, Nandi P, Mazumder R and Kar R 2015 Tectonostratigraphic evolution of the Nellore schist belt, southern India, since the Neoarchaean; *Geol. Soc. London Memoir* **43** 269–282.

Saha D, Patranabis-Deb S and Collins A 2016 Proterozoic stratigraphy of southern India cratons and global context; *Stratigraphy and Timescales* **1** 1–59.

Sain A, Saha D, Joy S, Jelsma H and Armstrong R 2017 New SHRIMP age and microstructures from a deformed A-type granite, Kanigiri, Southern India: Constraining the hiatus between orogenic closure and post-orogenic rifting; *J. Geol.* **125(2)** 241–259.

Santosh M, Yokoyama K and Acharyya S K 2004 Geochronology and tectonic evolution of Karimnagar and Bhopalpatnam granulite belts, central India; *Gondwana Res.* **7** 501–518.

Sharma R S 2009 *Cratons and fold belts of India*; Springer, Berlin.

Sheppard S, Rasmussen B, Zi J W, Somasekhar V, Sarma S D, Mohan R M, Krapež B, Wilde S A and McNaughton N J 2017 Sedimentation and magmatism in the Paleoproterozoic Cuddapah basin, India: Consequences of lithospheric extension; *Gondwana Res.* **48** 153–163.

Upadhyay D 2008 Alkaline magmatism along the southeastern margin of the Indian shield: Implications for regional geodynamics and constraints on craton – Eastern Ghats Belt suturing; *Precamb. Res.* **162** 59–69.

Upadhyay D, Gerdes A and Raith M M 2009 Unravelling sedimentary provenance and tectonothermal history of high-temperature metapelites, using zircon and monazite chemistry: A case study from the Eastern Ghats Belt, India; *J. Geol.* **117** 665–683.

Vadlamani R 2010 Palaeoproterozoic (1.9 Ga) extension and breakup along the eastern margin of the Eastern Dharwar Craton, SE India: New Sm–Nd isochron age constraints from anorogenic mafic magmatism in the Neoarchean Nellore greenstone belt; *J. Asian Earth Sci.* **37** 67–81.

Vadlamani R, Kröner A, Vasudevan D, Wendt I, Tobschall H and Chatterjee C 2012 Zircon evaporation ages and geochemistry of metamorphosed volcanic rocks from the Vinjamuru domain, Krishna Province: Evidence for 1.78 Ga convergent tectonics along the southeastern margin of the Eastern Dharwar Craton; *Geol. J.* **48** 293–309.

Van Achterbergh E, Ryan C G, Jackson S E and Griffin W L 2001 LA-ICP-MS in the earth sciences: Appendix 3, data reduction software for LA-ICP-MS; In: *Short course Mineralogical Association of Canada* (ed.) Sylvester P J, pp. 239–243.

Vansutre S and Hari K R 2010 Granulite belts of central India with special reference to the Bhopalpatnam Granulite Belt: Significance in crustal evolution and implications for Columbia supercontinent; *J. Asian Earth Sci.* **39** 794–803.

Vansutre S, Hari K R and Vishwakarma N 2013 Implications of geochemistry in support of Palaeo-Proterozoic tectonothermal evolution of Bhopalpatnam Granulite Belt, Bastar Craton, Central India; *J. Geol. Soc. India* **81** 503–513.

Vijaya Kumar K and Leelanandam C 2008 Evolution of the Eastern Ghats Belt, India: A plate tectonic perspective; *J. Geol. Soc. India* **72** 720–749.

Vijaya Kumar K, Ernst W G, Leelanandam C, Wooden J L and Grove M J 2010 First Paleoproterozoic ophiolite from Gondwana: Geochronologic–geochemical documentation of ancient oceanic crust from Kandra, SE India; *Tectonophys.* **487** 22–32.

Vijaya Kumar K, Leelanandam C and Ernst W G 2011 Formation and fragmentation of the Palaeoproterozoic supercontinent Columbia: Evidence from the Eastern Ghats Granulite Belt, southeast India; *Int. Geol. Rev.* **53** 1297–1311.

Wang Y, Fan W, Zhao G, Ji S and Peng T 2007 Zircon U–Pb geochronology of gneissic rocks in the Yunkai massif and its implication on the Caledonian event in the South China block; *Gondwana Res.* **12** 404–416.

Wang X, Griffin W L, Chen J, Huang P and Li X 2011 U and Th contents and Th/U ratios of zircons in felsic and mafic magmatic rocks: Improved zircon melt distribution coefficients; *Acta Geol. Sinica* **85** 164–174.

Yoshida M, Bindu R S, Kagami H, Rajesham T, Santosh M and Shirahata H 1996 Geochronologic constraints of granulite terranes of South India and their implications for the Precambrian assembly of Gondwana; *J. Southeast Asian Earth Sci.* **14** 137–147.

Zhang J, Mattinson C G, Meng F, Wan Y and Tung K 2008 Polyphase tectonothermal history recorded in granulitized gneisses from the north Qaidam HP/UHP metamorphic terrane, Western China: Evidence from zircon U–Pb geochronology; *Geol. Soc. Am. Bull.* **120** 732–749.

Corresponding editor: N V CHALAPATHI RAO